Eindhoven University of Technology

MASTER

Modeling of micro-discharges

Hagelaar, G.J.M.

Award date:
1996

Link to publication

Disclaimer
This document contains a student thesis (bachelor's or master's), as authored by a student at Eindhoven University of Technology. Student theses are made available in the TU/e repository upon obtaining the required degree. The grade received is not published on the document as presented in the repository. The required complexity or quality of research of student theses may vary by program, and the required minimum study period may vary in duration.

General rights
Copyright and moral rights for the publications made accessible in the public portal are retained by the authors and/or other copyright owners and it is a condition of accessing publications that users recognise and abide by the legal requirements associated with these rights.

- Users may download and print one copy of any publication from the public portal for the purpose of private study or research.
- You may not further distribute the material or use it for any profit-making activity or commercial gain

Eindhoven University of Technology
Department of Applied Physics
Elementary Processes in Gas discharges

MODELING OF MICRO-DISCHARGES

Gerjan Hagelaar
VDF/NG 96-09

december 1996

graduation report
supervision: dr. T. Hbid

Abstract

ABSTRACT

The aim of this graduation work is the study of micro-discharges by means of numerical modeling. Micro-discharges are gas discharges on a scale of hundreds of micrometers and they are used in many flat panel display technologies. In order to learn more about the mechanisms underlying the behavior of these discharges, a one dimensional multi-fluid model has been developed. The computer code of this model self-consistently solves a system of equations consisting of moments of the Boltzmann equation and the Poisson equation, using the explicit method. An exponential scheme is used for the solution the moments of the Boltzmann equation. We concentrate on DC micro-discharges and afterglows in pure helium and helium-nitrogen mixtures. Models for the reaction kinetics of these gases have been obtained by means of an investigation of the literature. We study the influence of several discharge parameters like gas pressure, applied voltage, and secondary emission coefficients on steady state particle densities and reaction rates, as well as density decay times in the afterglow. The results support classical ideas about DC discharges and agree with experimental measurements on a display panel.

SAMENVATTING

Het doel van dit afstudeerwerk is het bestuderen van micro-ontladingen door middel van numerieke modellering. Micro-ontladingen zijn gasontladingen op een schaal van enkele honderden micrometers en ze worden toegepast in tal van platte beeldbuis-technologieën. Om inzicht te krijgen in de fysische mechanismen die ten grondslag liggen aan het gedrag van deze ontladingen is een ééndimensionaal vloeistofmodel ontwikkeld. De computer-code van dit model berekent via de expliciete methode een zelfconsistente oplossing van een systeem van vergelijkingen, bestaande uit momenten van de Boltzmann-vergelijking en de Poisson-vergelijking. Voor het oplossen van de momenten van de Boltzmann-vergelijking wordt een exponentieel schema gebruikt. We richten ons op DC micro-ontladingen en afterglows in puur helium en helium-stikstof mengels. Met behulp van literatuuronderzoek zijn modellen opgesteld voor de reactiekinetiek van deze gassen. We bestuderen de invloed van diverse ontladingsparameters zoals gasdruk, electrode-spanning, en secundaire emissie-coefficiënten op zowel de deeltjesdichtheden en reactiesnelheden in de steady state, als de vervaltijden voor de deeltjesdichtheden in de afterglow. De resultaten ondersteunen klassieke ideeën over DC gasontladingen en komen overeen met de resultaten van metingen aan een proefpaneel.

Table of contents

TABLE OF CONTENTS

Abstract 3
Samenvatting 3
Table of contents 5

1 Introduction 7

1.1 Display panels 7
1.2 PALC operation principle 7
1.3 Numerical modeling 9
1.4 A fully developed DC glow discharge 10
1.5 Afterglow 14

2 The model 17

2.1 The fluid approximation 17
2.2 The system of coupled equations 21
2.3 Calculating densities: the exponential scheme 23
2.4 Boundary conditions for the flux 25
2.5 Solving the energy equation 26
2.6 Calculating the electric field 26
2.7 The time step and spatial step 28
2.8 Input data for the model 29

3 Species and reactions 33

3.1 Kinetic models 33
3.2 Pure helium 33
3.3 Helium-nitrogen mixtures 36
3.4 Data 38

4 Results and conclusions 47

4.1 A DC discharge in pure helium 47
4.2 Influences of parameters 51
4.3 DC discharges in helium-nitrogen mixtures 56
4.4 Afterglow 59
4.5 Addressing and afterglow 64
4.6 Comparison to experimental results 66
4.7 Scaling 68

5 General conclusions 73

Appendix 75

A Gauss elimination 75
B Cross-sections 76

Technology assesment 79
References 81

1 INTRODUCTION

1.1 DISPLAY PANELS

In this report we present a one dimensional model for micro-discharges. Micro-discharges are glow discharges on a very small scale. The distance between the electrodes is typically a few hundreds of micrometers and the gas pressure is relatively high, several hundreds of Torrs. These kinds of discharges are very interesting in connection with the newest generation of display panels. Micro-discharges have several properties that make them suitable for use in display panels. First, they can be switched on and off very quickly. Furthermore, they can emit light. There are several technologies for flat panel displays that make use of micro-discharges.

Best known are the Plasma Display Panels (PDP's). In this technology the light emitted by the plasma is used to constitute the image on the screen. A PDP consists of a matrix of small discharge cells. Every pixel has its separate micro-discharge with its own emissive intensity. In monochrome PDP's the visual light from the discharges is used directly, whereas in color PDP's the ultraviolet light is used to excite phosphors, which emit visible light in turn. One can distinguish between AC and DC PDP's. In AC PDP's the electrodes are insulated from the plasma and the discharge is capacitively induced, whilst in DC DPD's the electrodes are in direct contact with the plasma and there is a continuous dc transport of charge.

A totally different technology is the Plasma Addressed Liquid Crystal technology (PALC) [BUZ90] [BUZ93a] [BUZ93b]. In PALC only the excellent switching characteristics of micro-discharges are used, the emitted light plays no part (a strong emission of light is even undesirable). The charges produced in the discharge are used to charge a liquid crystal layer, and thus regulate the transparency of this layer. The light in the display panel comes from a constant back-lighting.

In this work we will concentrate on the study of micro-discharges as used in PALC. This is very interesting, because up till now, extensive research has been done only on PDP-discharges. Most micro-discharge modeling efforts concern AC PDP-discharges, while very little is know about the PALC-discharges.

1.2 PALC OPERATION PRINCIPLE

A PALC display panel consists of a large number of parallel channels that are filled with gas. The channels are made of transparent material (glass) so that they let through the light of the back-lighting. Every channel constitutes a horizontal line of the display panel. The width of such a channel is 300-500 μm and its depth about 100 μm. The channel length is of course equal to the width of the panel. A liquid crystal layer is situated on the top of the channels. On the bottom of each channel, there are two very long and thin parallel electrodes (along the direction of the channel). The gap between these electrodes is 200-400 μm. On the top of the liquid crystal layer, a large number of also very long and thin and mutually parallel electrodes is located, perpendicular to the direction of the channels (data-electrodes). These data-electrodes are also made of transparent material, and they correspond to the vertical columns of the display panel.

A discharge is created in one of the channels, by applying a voltage pulse of several hundreds of Volts to the electrodes of the channel in question. During this discharge pulse the strong electric field accelerates the electrons in the gas to such high velocities, that they can ionize gas particles and produce new free electrons. The electron and ion densities increase until an equilibrium is reached between creation (ionization) and loss processes (mainly drift and diffusion to the walls of the channel). After this equilibrium has been reached the voltage is switched back to zero. Such a discharge pulse typically lasts a few microseconds. After the pulse the electrons are no longer accelerated by the field and their mean velocity decreases rapidly. As a result ionization becomes very unlikely and the plasma in the channel perishes. This stage is usually called the afterglow.

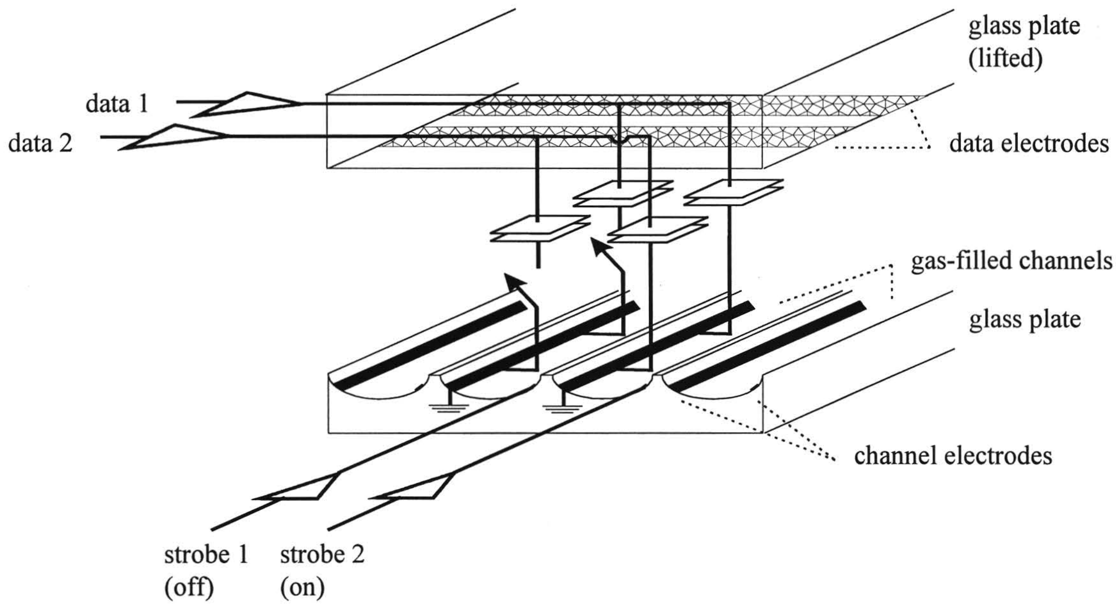

Figure 1.1: Open PALC panel with a schematic representation of its electronic behavior. The capacitors represent the liquid crystal layer.

Before the plasma has disappeared, a part of the charged particles is pulled to the surface of the liquid crystal layer, by application of certain voltages between (one of) the channel electrodes and the data electrodes. Of course, every data electrode is addressed with its own voltage, so this effect varies along the channel. The addressing voltages are rather low, and they produce an electric field in the liquid crystal layer and in the channel. This field is so weak that it cannot produce or sustain a discharge, it just pulls charges to the surface of the liquid crystal layer. As a consequence, the layer is charged like a capacitor, till the total addressing voltage is across the layer. This results in a certain transparency of the liquid crystal layer. The addressing of the data electrodes can start either during or just after the discharge pulse. The only thing that matters, is that there are many charged particles in the channel. The data addressing can be stopped if the plasma has vanished in the late afterglow. The channel is then an insulator, so that the charges on the layer cannot go anywhere and the layer will remain charged. Now a discharge pulse is applied to the next channel, and the procedure is repeated. By going down the discharge channels like this, each time producing a discharge and addressing, we can build an image line by line. The idea is that only the line with a plasma in its channel will display the data of the data electrodes. The other lines do not respond to the addressing and will maintain the image they had.

The technology makes some demands on the micro-discharges in the channels. There must be sufficient charged particles to charge the liquid crystal layer. It is also important that the afterglow lasts not too long. Nearly all charged particles must have disappeared before the next line is addressed, otherwise the image of the line will be (partially) lost (the layer will discharge again) or be influenced by the data of the next line. The latter is called cross-talk between lines. Further demands are imposed by a certain requested lifetime of a display panel. The channel electrodes are in direct contact with the plasma and are therefore liable to corrosion by the plasma. All these demands must absolutely be satisfied to make the PALC technology feasible at all. Moreover, one has to take into account commercial aspects of a display panel. Production costs and power consumption should be as low as possible.

There are many parameters that one can control to influence or even determine the micro-discharges, such as the composition of the gas, the gas pressure, the height of the discharge pulse voltage, the duration of the discharge and data pulses, the electrode material and possibly coating, the size and shape of the electrodes, the geometry of the discharge channel, etc., etc. In order to optimize these parameters for the demands on the discharge, is it necessary to understand and to be able to predict their influence.

1.3 NUMERICAL MODELING

The micro-discharges in the channels are so small that it is hard to study them experimentally. Producing PALC test panels and building experimental setups to study them is an expensive and time-consuming affair. It is possible to measure discharge and afterglow currents and intensities of emitted light, but it is nearly impossible to do measurements that provide a detailed image of the structure of the discharge. Experimental results do hardly provide any insight in the mechanisms that take place in a micro-discharge but represent mainly a macroscopic outcome of these mechanisms. In order to explain and understand the behavior of micro-discharges one usually has to resort to analogies with discharge phenomena of larger dimensions. These larger discharges can be studied more easily and are nowadays quite well understood. For most kinds of discharges scaling laws can be derived, but is it uncertain to what extend these scaling laws are valid for really extreme scalings over orders of magnitude.

An alternative way to obtain an insight in what happens in micro-discharges is given by numerical modeling. In numerical modeling all fundamental laws and processes that are known or suspected to play part in a discharge are implemented into a computer code. Subsequently this computer code calculates the resulting situation. If the numerical model is good, the final modeling result represents a physical situation and corresponds to experimental measurements. In this report we present such a numerical model for discharges and we apply it to the PALC configuration. To describe the PALC configuration in a proper way, the numerical model should take into account at least two spatial dimensions. However, building a two dimensional model is a very complicated matter with many hooks and eyes to it. Moreover, two dimensional calculations may take lots of calculation time, which is very inconvenient. We therefore confine ourselves to a one dimensional model. Although such a model is incapable of exactly representing the PALC situation, it can give us useful insights and approximations. (Moreover, creating a one dimensional model is a necessary step in the development of a two dimensional model. With the insights gained by this work we will be able to build a two dimensional model in the future.)

1.4 A FULLY DEVELOPED DC GLOW DISCHARGE

In this section we will discuss, in a somewhat phenomenological way, a fully developed decent current glow discharge. This is useful in order to introduce some necessary concepts and to give an idea about the mechanisms governing DC discharges. The configuration we will consider is that of two parallel flat plate electrodes, which are big compared to the distance between them. In describing such a configuration, the only direction of importance is the direction perpendicular to the electrodes. This means that a one dimensional description is appropriate for this configuration. (It is the physical situation corresponding to a one dimensional model). Between the electrodes there is a gas at a certain pressure. This gas is partially ionized. We consider here the case that there is only one kind of ion, a univalent positively charged one.

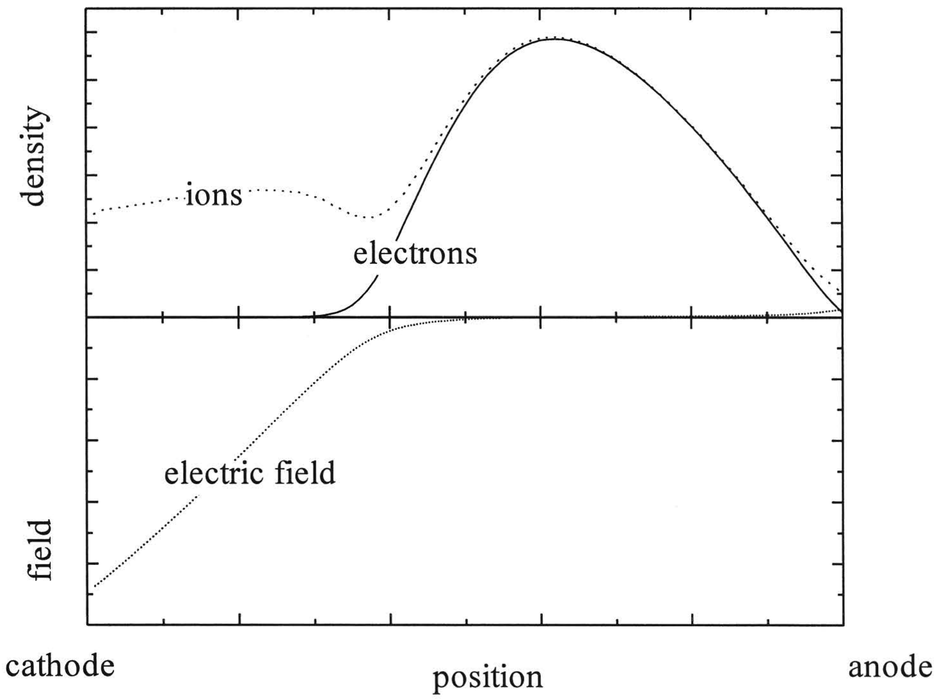

Figure 1.2: Typical electron and ion density distributions in a steady state DC glow discharge. These distributions have been obtained with the numerical model presented in this report.

In DC glow discharges the voltage needed to sustain the discharge amounts to several hundreds of Volts. This voltage produces an electric field between the electrodes, which accelerates the electrons towards the anode (positive electrode) and the ions towards the cathode (negative electrode). The acceleration by the field is resisted by elastic collisions with neutral gas particles. Time after time the charged particles gain velocity by the field and lose it in elastic collisions. The macroscopic result is that the electrons and ions are not accelerated, but have constant velocities, which are called drift velocities. The electrons drift towards the anode and the ions towards the cathode. The drift velocity of the electrons is about two orders of magnitude bigger than the drift velocity of ions. This difference in drift velocity gives rise to the development of space charges which strongly influence the externally applied electric field. A typical situation is depicted in Figure 1.2.

It is obvious that the discharge can be divided into two regions. In front of the cathode there is a region in which the electron density is very small compared to the ion density. Such a region is generally called a sheath. The positive space charge of this sheath screens the remainder of the discharge from the electric field. Almost the entire potential difference of the electrodes is across the sheath region. It is therefore also called the cathode fall. The remainder of the discharge consists of a plasma, in which the densities of electrons and ions are equal to each other. The electric field in this plasma is relatively low. The classical name for this region is "glow region".

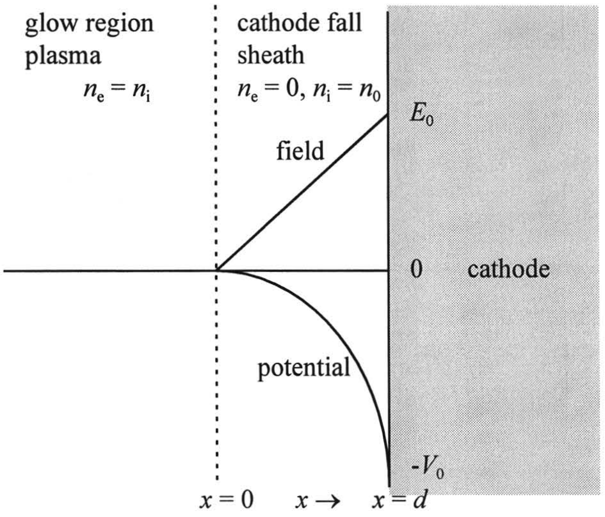

Figure 1.3: Schematic representation of the cathode fall region.

We will now perform some straightforward calculations to demonstrate the relationships between different mechanisms in the discharge. In order to make this possible, we need to make drastic simplifications. The equations we will derive will therefore only have an illustrative value. We use the simplified representation of the cathode fall shown in Figure 1.3. Assume that the ion density in the cathode fall has a constant value n_0 and that the electron density is negligible compared to this. The position x increases from anode to cathode and is zero at the boundary between the plasma and the cathode fall. The thickness of the cathode fall region is d, so the cathode is located at $x = d$. The anode is grounded and the cathode has a negative potential $-V_0$. Assume that the potential at $x = 0$ is equal to the anode potential. The relationship between the electric potential V and the space charge is given by the Poisson equation

$$\frac{\mathrm{d}^2 V(x)}{\mathrm{d}x^2} = -\frac{\rho(x)}{\varepsilon_0} = -\frac{e n_0}{\varepsilon_0} \tag{1.1}$$

The space charge density in the cathode fall ρ is constant and equal to $\rho = en_0$. Integrating this equation once gives the electric field E

$$E(x) = -\frac{\mathrm{d}V}{\mathrm{d}x} = \frac{en_0}{\varepsilon_0}x \tag{1.2}$$

Integrating again gives the potential

$$V(x) = -\frac{en_0}{2\varepsilon_0}x^2 \tag{1.3}$$

At $x = d$ this potential must be equal to $-V_0$. If we substitute these values, we obtain

$$n_0 = \frac{2\varepsilon_0}{e}\frac{V_0}{d^2} \tag{1.4}$$

The electric field at the cathode ($x = d$) is then

$$E_0 = 2\frac{V_0}{d} \tag{1.5}$$

The ions the cathode fall are transported towards the cathode by the electric field. The ion drift velocity W_i depends on the electric field and on the gas pressure. In general, it is a function of the ratio of the electric field and the pressure E/p. This ratio is called the reduced electric field. The ion drift flux φ_0 towards the cathode (at $x = d$) is equal to

$$\varphi_0 = W_\mathrm{i}\left(E_0/p\right)n_0 \tag{1.6}$$

the brackets indicate the dependence of W_i on the reduced field E/p. For most ions it is known that for high values of the reduced electric field ($E/p > 100$), which typically occur in front of the cathode, the drift velocity increases as the square root of the reduced field. Using this fact and equations (1.4) and (1.5), we can derive the following relationship

$$\varphi_0 \propto \sqrt{\frac{E_0}{p}}n_0 \propto \frac{V_0^{3/2}}{p^{1/2}d^{5/2}} \tag{1.7}$$

The ions arriving at the cathode are neutralized by the free metal electrons of the cathode. The energy released by these recombination processes can be used to emit an electron from the cathode material. This phenomenon is called secondary emission and it is absolutely necessary to sustain a DC discharge, as we will see soon. The secondary emission is characterized by a secondary emission coefficient γ, which is defined as the average number of electrons that are emitted per incident ion. This secondary emission coefficient depends largely on the combination of ion species and electrode material and is usually in the range from $\gamma = 0.01$ to $\gamma = 0.1$. The current density through the cathode is the result of the ion flux towards the cathode and the secondary emission and is given by

$$J = (1+\gamma)e\varphi_0 \propto \frac{(1+\gamma)V_0^{3/2}}{p^{1/2}d^{5/2}} \tag{1.8}$$

In a stationary situation, the disappearance of every ion at the cathode is compensated for by the creation of an ion in the discharge. We will assume here that the only creation process for ions is direct ionization of gas particles by electron impact. Because these processes require a high electron energy, they occur mainly in the cathode fall, where the strong electric field heats the electrons. The ionizations in the cathode fall are caused by the secondary electrons, the electrons that are emitted from the cathode by ion impact and cross the cathode fall at high drift velocity. During their crossing of the cathode fall the secondary electrons have to cause enough ionizations to make up for the loss of ions at the cathode. If the secondary emission coefficient is equal to γ, then every secondary electron must cause $1/\gamma$ ionizations.

The rate of electron impact ionization processes can be described by the quantity α, which is defined as the number of ionizations by one electron per unit of traveled distance. Suppose that this α is constant along the electron path through the cathode fall and that $\alpha = 0$ in the plasma. The number of ionizations of one secondary electron is then equal to αd. The electrons produced in these ionizations start to cause ionizations themselves. This results in a true "electron avalanche". On each ionization of the secondary electron, the total number of electrons in the avalanche doubles. By the time that the secondary electron reaches the plasma (and stops ionizing), the number of electrons in the avalanche amounts to $2^{\alpha d}$. The total number of ionizations caused by one secondary electron is then $2^{\alpha d}$-1. This number must be equal to $1/\gamma$

$$2^{\alpha d} - 1 = \frac{1}{\gamma} \tag{1.9}$$

This equation can be rearranged into an expression for the thickness of the cathode fall

$$d = \frac{\ln\left(\frac{1}{\gamma}+1\right)}{\alpha \ln 2} \tag{1.10}$$

In general the coefficient α is proportional to the density of the gas particles, i.e. gas pressure p. Using this fact in equation (1.10), we obtain

$$d \propto \frac{\ln\left(\frac{1}{\gamma}+1\right)}{p} \tag{1.11}$$

This means that we can control the size of the cathode fall by regulating the gas pressure. There is experimental evidence that reciprocal proportionality of d and p is valid not only under our assumptions but in a wide range of conditions [RAI91]. Notice that for a DC glow discharge it is absolutely required that the size of the cathode fall is smaller than the distance between the electrodes. If this requirement is not met, the discharge cannot be sustained or we get a different kind of discharge with a different structure of densities and fields. This fact gives rise so-called "scaling laws" or "similarity laws". If we decrease the distance between the electrodes by a factor a, we will have a "similar" discharge if we increase the pressure by a factor a^{-1}, i.e. we must keep the product of pressure and electrode distance constant. The reduced electric field E/p is another quantity that is kept constant in scaling DC discharges. (Combine relations (1.2), (1.4) and (1.11).)
If we use the relation (1.11) in (1.8) we obtain

$$J \propto \frac{1+\gamma}{\left(\ln\left(1+\frac{1}{\gamma}\right)\right)^{5/2}} p^2 V_0^{3/2} \tag{1.12}$$

The current through the discharge can be controlled by regulating the pressure and the applied voltage. In the scaling of discharges with a scale factor a, the current density behaves as a^{-2}. In practice it is useful (if not necessary) to place a (current limiting) resistor in series with the discharge, in order achieve a stable DC glow discharge. This gives an additional coupling between the voltage over the discharge V_0 and the current J. (We cannot regulate V_0 directly in this case.)

1.5 AFTERGLOW

In this section we will describe what happens to the discharge described in the preceding section if we switch off the sustaining voltage between the electrodes. The electric fields in the discharge will vanish rapidly, the space charges and the cathode fall will disappear, and the drift of ions and electrons stops. Moreover, the electrons are no longer heated by the field and cool down to the gas temperature so that they can no longer cause ionizations. The densities of electrons and ions start to decrease, mainly due to diffusion to the electrodes. We did not take into account diffusion in our discussion of the discharge itself, but in the afterglow this phenomenon comes to the fore. The diffusion is governed by the Fick law

$$\varphi = -D\frac{\mathrm{d}n}{\mathrm{d}x} \tag{1.13}$$

which says that the flux φ of particles due to diffusion is oppositely directed and proportional to the gradient of their density. The proportionality constant D is called the diffusion coefficient. Ions and electrons each have their own diffusion coefficient. The diffusion coefficient of electrons is much bigger than that of ions, so that the electron density tends to decrease much faster than the ion density. However, this immediately leads to the development of positive space charges, which produce a small electric field (the ambipolar field) that works against the electron diffusion and helps the diffusion of the ions. Because the electrons and the ions are coupled to each other by means of electrical forces, they do not diffuse separately but they diffuse together with a diffusion coefficient that is somewhere in between their free diffusion coefficients. This phenomenon is called “ambipolar” diffusion. Let us now make a basic calculation to see the development of the electron and ion densities under the influence of ambipolar diffusion. For this purpose we will redefine our position variable x in a symmetrical way, assigning $x = 0$ to the position exactly midway between the electrodes. The electrodes are located at $x = 1/2\ L$ and $x = -1/2\ L$, with L the distance between the electrodes. Assume that no particles are created or lost in collisions. We can write down the continuity equation

$$\frac{\partial n}{\partial t} + \frac{\partial \varphi}{\partial x} = 0 \tag{1.14}$$

n and φ are the density and flux of either ions or electrons.
The flux φ is due to ambipolar diffusion

$$\varphi = -D_{\text{amb}} \frac{\partial n}{\partial x} \tag{1.15}$$

with D_{amb} the ambipolar diffusion coefficient. Substituting this equation in equation (1.14) yields

$$\frac{\partial n}{\partial t} = D_{\text{amb}} \frac{\partial^2 n}{\partial x^2} \tag{1.16}$$

A symmetric solution of this differential equation is given by

$$n(x,t) = n(0,0) \cos\left(\frac{x}{\Lambda}\right) \exp\left(-\frac{t}{\tau}\right) \tag{1.17}$$

with

$$\Lambda^2 = D_{\text{amb}} \tau \tag{1.18}$$

$n(0,0)$ is the density in the middle between the electrodes at $t = 0$. Λ and τ are called the characteristic diffusion length and time, respectively. Their values are determined by the boundary conditions. We will not go into the exact boundary conditions here, but what they come down to is that it is a good approximation to take the densities zero at the boundaries. Setting n to zero at $x = 1/2\ L$ leads to

$$\tau = \frac{L^2}{\pi^2 D_{\text{amb}}} \tag{1.19}$$

(Λ can be calculated from this result by using equation (1.18).) We see that densities governed by diffusion develop a sinusoidal profile with a maximum in the middle and zero at the electrodes. The densities decay in an exponential way.

Ambipolar diffusion does not occur in all circumstances. If the density of electrons and ions becomes to low, the ambipolar field becomes too weak to prevent the electrons from diffusing away and leaving the ions behind. We can make an estimation of this density at which the ambipolar diffusion breaks. The typical distance at which deviations from quasi-neutrality can exist is given by the Debye length

$$l = \sqrt{\frac{\varepsilon_0 k T_\mathrm{e}}{e^2 n}} \tag{1.20}$$

with T_e the electron temperature and k the Boltzmann constant. The ambipolar field is produced in a region with the size of this Debye length. The ambipolar diffusion cannot be maintained if the Debye length is larger than the half of the distance between the electrodes. For an electron temperature of 300 K this means that ambipolar diffusion can only arise if

$$n > \frac{8.5 \times 10^7}{L^2} \tag{1.21}$$

with n in cm^{-3} and L in cm.

2 THE MODEL

2.1 THE FLUID APPROXIMATION

The ideal way to describe a plasma is to solve the equation of motion and the Maxwell equations for every individual particle within the plasma. Since we are dealing with enormous amounts of particles, this is of course impossible to do. We have to resort to other means of mathematical description. For large numbers of particles, the fluid approximation is very useful. Particles are not followed individually, but are described in terms of macroscopic, microscopically averaged quantities, such as particle density and flux. For a plasma, consisting of many different species of particles (atoms or molecules, ions, electrons), we need a multifluid description. Every species is to be regarded as a separate fluid, with its own density and flux at each spatial point. The different fluids are coupled by means of electric forces and by the processes occurring between particles of different species. In this section we will give a mathematical description of a such fluid.

For a fluid we can write down the so-called Boltzmann equation

$$\frac{\partial f}{\partial t} + \mathbf{v} \cdot \nabla_{\mathbf{r}} f + \mathbf{a} \cdot \nabla_{\mathbf{v}} f = \left(\frac{\partial f}{\partial t} \right)_{\mathrm{col}} \tag{2.1}$$

This is a kind of continuity equation in the six dimensional phase space. The function $f(\mathbf{r},\mathbf{v},t)$ is the six dimensional particle density, and $f\Delta\mathbf{r}\Delta\mathbf{v}$ is equal to the number of particles with a position between $\mathbf{r}$ and $\mathbf{r}+\Delta\mathbf{r}$ and a velocity between $\mathbf{v}$ and $\mathbf{v}+\Delta\mathbf{v}$. The term on the right denotes the change in f due to production or loss of the particles considered in collisions. The vector $\mathbf{a}(\mathbf{r},\mathbf{v},t)$ is the acceleration. For a charged particle fluid (electrons or ions) this $\mathbf{a}$ is given by

$$\mathbf{a} = \frac{q}{m}(\mathbf{E} + \mathbf{v} \times \mathbf{B}) \tag{2.2}$$

the Lorenz force over the mass. **E** and **B** indicate the electric and magnetic fields, q and m give the particle charge and mass.

The Boltzmann equation in phase space is very complicated and hard to handle. It can be solved numerically, but only if the electric and magnetic fields are constant in time. To use the Boltzmann equation in time and space varying fields, we have to make simplifications. This can be done by integrating it over all velocities. By doing so we do not directly take into account the velocity distribution of the particles any more. We only use their spatial density distribution $n(\mathbf{r},t)$

$$n(\mathbf{r},t) = \int_{\mathbf{v}} f(\mathbf{r},\mathbf{v},t) \mathrm{d}^3\mathbf{v} \tag{2.3}$$

and their mean velocity

$$\overline{\mathbf{v}}(\mathbf{r},t)=\frac{1}{n(\mathbf{r},t)}\int_{\mathbf{v}}\mathbf{v}f(\mathbf{r},\mathbf{v},t)\mathrm{d}^3\mathbf{v} \tag{2.4}$$

This principal of integrating out the velocity distribution is used by the so-called moment method. Using this method, we multiply the Boltzmann equation by a certain power of the velocity **v** and then integrate it over all velocities. For every power of **v** (1, **v**, **v**·**v** etc.) used, we get a new differential equation in three dimensions, which is called a moment. In each moment a new quantity appears, which can be calculated using the next moment. The whole infinite set of moments is equivalent to the Boltzmann equation itself. A simplification of the Boltzmann equation can now be easily made by taking into account only a limited number of moments. To close the system at a given moment, we need to posit a relation for the new quantity arising in this moment. This will all be clarified below, where we will work out the moment method.

We find the zeroth moment by multiplying equation (2.1) by 1 ($=\mathbf{v}^0$), and integrating over velocity space

$$\frac{\partial n}{\partial t}+\nabla_{\mathbf{r}}(n\overline{\mathbf{v}})=\int_{\mathbf{v}}\left(\frac{\partial f}{\partial t}\right)_{\mathrm{col}}\mathrm{d}^3\mathbf{v}\equiv S \tag{2.5}$$

This is just the continuity equation. $S(\mathbf{r},t)$ is the source term and gives the number of particles created or lost per unit volume and per unit time at position **r** and time *t*. The second term on the left gives the divergence of the particle flux. To solve the density, we need to know the this flux. It can be calculated from the first moment (multiply (2.1) by *m***v** and integrate)

$$\frac{\partial nm\overline{\mathbf{v}}}{\partial t}+nm\left(\overline{\mathbf{v}}\cdot\nabla_{\mathbf{r}}\right)\overline{\mathbf{v}}+\overline{\mathbf{v}}\left(\nabla_{\mathbf{r}}\cdot nm\overline{\mathbf{v}}\right)+\nabla_{\mathbf{r}}:\underline{\underline{\mathbf{P}}}-n\overline{\mathbf{F}}=\int_{\mathbf{v}}m\mathbf{v}\left(\frac{\partial f}{\partial t}\right)_{\mathrm{col}}\mathrm{d}^3\mathbf{v} \tag{2.6}$$

This moment is called the momentum equation, for it describes the transport of momentum. **F** is the force exerted on the particles and is equal to *m***a**, where **a** is given by equation (2.2). The quantity $\underline{\underline{\mathbf{P}}}$ is the kinetic pressure tensor

$$\underline{\underline{\mathbf{P}}}=m\int(\mathbf{v}-\overline{\mathbf{v}})(\mathbf{v}-\overline{\mathbf{v}})f\mathrm{d}^3\mathbf{v} \tag{2.7}$$

The term on the right of equation (2.6) denotes the momentum lost (or gained) in collisions per unit volume per unit time. We can define a momentum transfer frequency ν_{m} (see Appendix B) to characterize this

$$\int_{\mathbf{v}}m\mathbf{v}\left(\frac{\partial f}{\partial t}\right)_{\mathrm{col}}\mathrm{d}^3\mathbf{v}=nm\overline{\mathbf{v}}\,\nu_{\mathrm{m}} \tag{2.8}$$

Using this definition and the continuity equation (2.5), we can rewrite the momentum equation as follows

$$nm\left(\frac{\partial}{\partial t}+\left(\bar{\mathbf{v}}\cdot\nabla_{\mathbf{r}}\right)\right)\bar{\mathbf{v}} = n\mathbf{F} - \nabla_{\mathbf{r}}:\underline{\underline{\mathbf{P}}} - Sm\bar{\mathbf{v}} + nm\nu_{\mathrm{m}}\bar{\mathbf{v}} \tag{2.9}$$

We will now make some approximations to simplify this equation.
If we suppose that

$$\frac{\partial\left(n\left|\bar{\mathbf{v}}\right|\right)}{\partial t} << n\left|\bar{\mathbf{v}}\right|\nu_{\mathrm{m}} \tag{2.10}$$

which is true for almost every practical situation, we can neglect the time derivative in the right term of equation (2.9). Further simplifications can be made by assuming that the systematic velocity $\bar{\mathbf{v}}$ is small compared to the thermal velocity $\mathbf{v}-\bar{\mathbf{v}}$, more precise

$$\bar{\mathbf{v}}\cdot\bar{\mathbf{v}} << \overline{\mathbf{v}\cdot\mathbf{v}} \tag{2.11}$$

In this case the kinetic pressure tensor (2.7) is diagonal and isotropic,

$$\underline{\underline{\mathbf{P}}} = \tfrac{1}{3}nm\overline{\mathbf{v}\cdot\mathbf{v}}\,\underline{\underline{\mathbf{I}}} = nkT\underline{\underline{\mathbf{I}}} \tag{2.12}$$

with T the temperature and $\underline{\underline{\mathbf{I}}}$ the unity tensor. (The physical interpretation of the fact that $\underline{\underline{\mathbf{P}}}$ is diagonal is that there is no viscosity.) Moreover, if (2.11) is the case, we can neglect the second part of the right term (inertia) and the term $-Sm\bar{\mathbf{v}}$ (compare (2.8) with the definition of S) of equation (2.9). Finally, we suppose that no magnetic field is present, like in the cases we are interested in here. Using these approximations and dividing by nm, the momentum equation becomes

$$n\bar{\mathbf{v}} = n\left(\frac{q}{m\nu_{\mathrm{m}}}\right)\mathbf{E} - \frac{1}{m\nu_{\mathrm{m}}}\nabla(nkT) \tag{2.13}$$

With the definitions of the drift velocity **W**

$$\mathbf{W} = \left(\frac{q}{m\nu_{\mathrm{m}}}\right)\mathbf{E} \tag{2.14}$$

and the diffusion coefficient D

$$D = \left(\frac{kT}{m\nu_{\mathrm{m}}}\right) \tag{2.15}$$

this is the well know drift diffusion equation. The first term is the flux due to the electric field (drift), and the second term gives the flux due to a concentration gradient (diffusion).
In the first moment (2.13) the particle temperature appears. We can calculate this temperature from the second moment but we can also close our system of moments now, assuming that there is a direct relationship between this temperature and the electric field. Such an assumption corresponds to the fact that at every position there is an equilibrium between the energy the particles gain per unit time by the electric field and the energy they lose per unit time in collisions. We will call this situation "local equilibrium". For heavier particle species (ions) the assumption of local equilibrium is justified, but for electrons we prefer to consider the second moment of the Boltzmann equation. This is obtained by multiplying equation (2.1) by $m\mathbf{v}\cdot\mathbf{v}$ and integrating over velocity space. Applying the approximations mentioned before, we get

$$\frac{\partial(n\bar{\varepsilon})}{\partial t}+\frac{5}{3}\nabla(n\bar{\varepsilon})\bar{\mathbf{v}}+\nabla\mathbf{Q}-qn\bar{\mathbf{v}}\cdot\mathbf{E}=-\nu_{\varepsilon}(n\bar{\varepsilon}) \tag{2.16}$$

This equation describes the energy transport. $\bar{\varepsilon}$ is the mean particle energy, and since we assumed that this energy is mainly due to random motion (2.11), it is equal to 3/2 kT. Analogously to ν_{m} in the momentum equation, we used here ν_{ε} the frequency for energy transfer in collisions. **Q** is the heat flux and it can be calculated from the third moment. However, we close our system here assuming that **Q** is proportional to the temperature gradient

$$\mathbf{Q}=\kappa\nabla(kT) \tag{2.17}$$

with the heat conductivity coefficient κ given by (see [RAI91])

$$\kappa=\frac{5}{2}Dn \tag{2.18}$$

Equation (2.17) can be written as follows

$$\mathbf{Q}=\frac{5}{2}Dn\nabla(kT)=\frac{5}{3}Dn\nabla\bar{\varepsilon}=\frac{5}{3}D\left(\nabla(n\bar{\varepsilon})-\bar{\varepsilon}\nabla n\right) \tag{2.19}$$

Inserting this relation and using the momentum equation (2.13), we can rewrite the energy equation

$$\frac{\partial(n\bar{\varepsilon})}{\partial t}+\nabla\cdot\left(\frac{5}{3}\mathbf{W}(n\bar{\varepsilon})+\frac{5}{3}D\nabla(n\bar{\varepsilon})\right)=qn\bar{\mathbf{v}}\cdot\mathbf{E}-\nu_{\varepsilon}(n\bar{\varepsilon}) \tag{2.20}$$

We will see later that this form of the energy equation is very convenient, because it looks so much like the continuity equation for particles. (In fact, it is the continuity equation for energy.)

2.2 THE SYSTEM OF COUPLED EQUATIONS

We describe the plasma by a multifluid model. In the glow discharges we are interested in the ionization degree is very low ($<10^{-5}$). There is also no gas flow. Therefore we can assume that the density and temperature of the neutral gas particles are constant in time and space. But for all the other particle species, like electrons, ions and possibly metastables, we have to calculate the particle densities as functions of time and position. Every species is to be regarded as a separate fluid, described by the moments of the Boltzmann equation. For every species p we have the continuity equation (2.5) and the momentum equation (2.13), in one dimension

$$\frac{\partial n_p}{\partial t}+\frac{\partial}{\partial x}\varphi_p = S_p \tag{2.21}$$

$$\varphi_p = W_p n_p - \frac{\partial}{\partial x}\left(D_p n_p\right) \tag{2.22}$$

the flux is indicated here by φ, and p can be electron, ion or metastable.
The drift velocity W can be written as

$$W_p = s_p \mu_p E \tag{2.23}$$

μ_p is called the mobility and is always defined positive (which is very inconvenient). Therefore we need to include a factor s_p which has the value -1 if p is a negatively charged particle and +1 otherwise. In general the mobility as well as the diffusion coefficient depend on the mean energy of the considered particle.
The source term S is determined by the reactions and processes occurring in the plasma, and it gives a coupling between the different fluids. S_p consists of positive contributions of the reactions in which a particle of species p is created and of negative contributions of the reactions in which such a particle is lost.

$$S_p = \sum_r N_{p,r} R_r \tag{2.24}$$

The index r refers to a reaction. $N_{p,r}$ is the net number of particles of species p created in one reaction of type r, and it can be negative as well as positive. R_r is the reaction rate of reaction r, i.e. the number of reactions happening per unit volume per unit time. This reaction rate is proportional to the densities of the reacting particles. The proportionality constant is called the reaction rate coefficient k_r. For a two particle reaction between species 1 and 2 we have $R = k{\cdot}n_1{\cdot}n_2$, for a three particle reaction $R = k{\cdot}n_1{\cdot}n_2{\cdot}n_3$. In general, the rate coefficient depends upon the energy of the particles involved. This is especially important if one of the particles is an electron. The reaction coefficient can then be heavily dependent not only on the electron temperature, but also on the electron energy distribution function.

For heavy particles, i.e. ions and metastable species, we make the assumption of local equilibrium (see Section 2.1). This means there is a direct relationship between the particle mean energy and the electric field, and drift velocity and diffusion coefficient can be regarded as functions of the electric field. For electrons this is not true. Electrons can gain energy by the field in one region where the field is strong and carry this energy to another region where the field weak. In order to know the electron mobility, the electron diffusion coefficient and the reaction coefficients of many important reactions (like ionization and excitation), it is therefore necessary to consider the energy equation (2.20) for electrons. In one dimension

$$\frac{\partial(n_e\bar{\varepsilon})}{\partial t}+\frac{\partial}{\partial x}\left(\frac{5}{3}W_e(n_e\bar{\varepsilon})+\frac{5}{3}D_e\frac{\partial}{\partial x}(n_e\bar{\varepsilon})\right)=-e\varphi_e E-\nu_\varepsilon(n_e\bar{\varepsilon}) \qquad (2.25)$$

The space charge densities in glow discharges are so big that they influence the electric field. This too gives a coupling between the fluids. Each charged particle fluid moves in an electric field influenced by itself and the other fluids. The relationship between the electric field and the charge density is described by the first Maxwell equation

$$\frac{\partial E}{\partial x}=\frac{\rho}{\varepsilon_0} \qquad (2.26)$$

where ρ is the charge density

$$\rho=\sum_p q_p n_p \qquad (2.27)$$

p again indicates a particle species and q_p is the charge of one particle of species p.

We have seen that all our equations are coupled to each other. To calculate the density of any particle species we need to know the electric field, the electron temperature and the densities of the other species. To calculate the electron energy, we also need to know the electric field. To calculate the electric field, we need to know all the densities. The equations (2.21), (2.22), (2.25), and (2.26) must be solved self-consistently. The method we use here to do this is called the explicit method. The densities of particles and electron energy and the electric field are calculated alternatively. Every iteration a small time-step is made. If for the solution of an equation we need to know a quantity that results from the solution of another equation, we just take this quantity from the solution of the preceding iteration. This uncouples the equations so that indeed we can solve all equations one by one.

The breakdown of a discharge cannot be simulated because our equations are not valid in this regime. Therefore we have to start our calculation from some assumed (not too small) density distribution for each particle species and for the electron temperature. After some time the calculation converges into a so-called steady state and is supposed to represent a real physical situation.

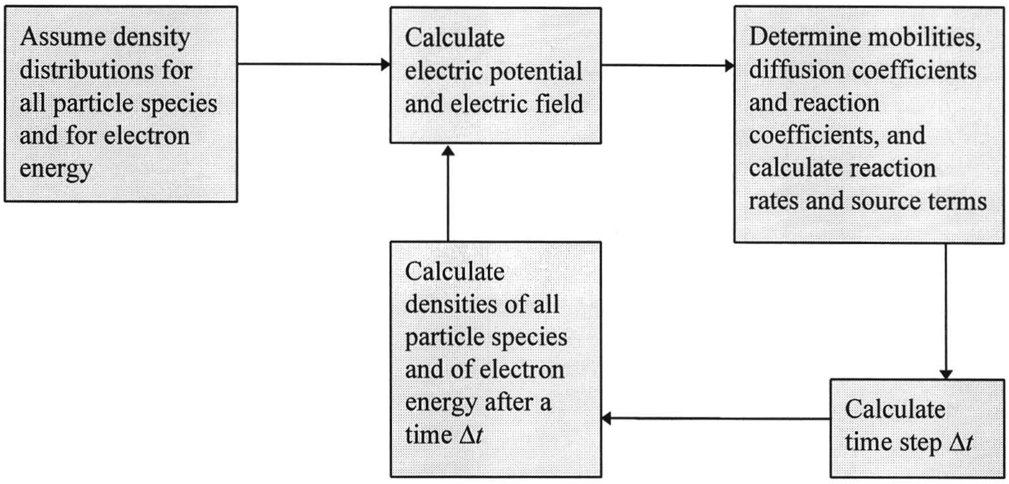
Assume density distributions for all particle species and for electron energy
Calculate electric potential and electric field
Determine mobilities, diffusion coefficients and reaction coefficients, and calculate reaction rates and source terms
Calculate time step Δt
Calculate densities of all particle species and of electron energy after a time Δt

Figure 2.1: Schematic representation of the explicit calculation method used by the model.

2.3 CALCULATING DENSITIES: THE EXPONENTIAL SCHEME

The particle densities are calculated from the continuity equation (2.21) and the momentum equation (2.22). The scheme used to solve these equations is an exponential scheme [BOE87] [SCH69]. It is robust and works under a wide range of conditions. We will describe the exponential scheme in this section. For convenience we drop the subscript p for the moment.

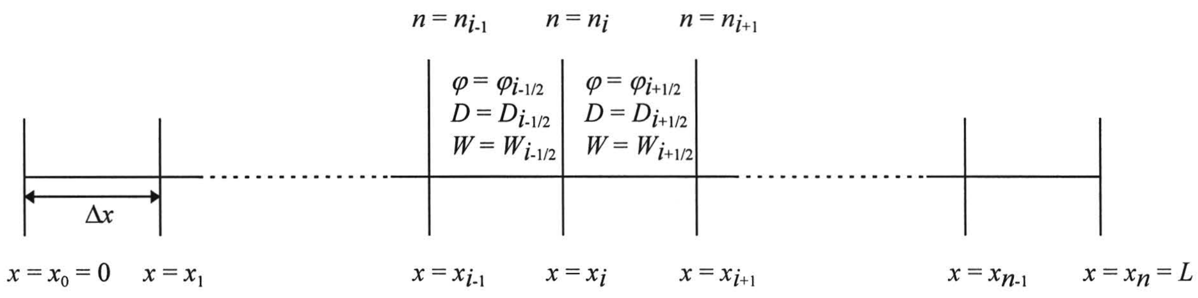
$n = n_{i-1}$
$n = n_i$
$n = n_{i+1}$
$\varphi = \varphi_{i-1/2}$
$D = D_{i-1/2}$
$W = W_{i-1/2}$
$\varphi = \varphi_{i+1/2}$
$D = D_{i+1/2}$
$W = W_{i+1/2}$
Δx
$x = x_0 = 0$
$x = x_1$
$x = x_{i-1}$
$x = x_i$
$x = x_{i+1}$
$x = x_{n-1}$
$x = x_n = L$

Figure 2.2: Definition of the grid.

The x-space from $x = 0$ to $x = L$ is divided into small intervals Δx. Define $x_i = i{\cdot}\Delta x$, a boundary between two intervals. We now suppose that within each interval the flux, the diffusion coefficient and the drift velocity are constant, i.e. independent of x. For the interval between x_i and x_{i+1}, we indicate the (constant) flux by $\varphi_{1+1/2}$, the diffusion coefficient by $D_{i+1/2}$ and the drift velocity by $W_{i+1/2}$. Within each interval the momentum equation

$$\varphi_{i+1/2} = W_{i+1/2}n(x) - \frac{\partial}{\partial x}\left(D_{i+1/2}n(x)\right) \qquad x_i \le x \le x_{i+1/2} \qquad (2.28)$$

can be solved analytically

$$n(x) = \frac{\varphi_{i+1/2}}{W_{i+1/2}} + C\exp\left(\frac{W_{i+1/2}}{D_{i+1/2}} x\right) \qquad x_i \le x \le x_{i+1/2} \tag{2.29}$$

where C is a constant. For given values of $D_{i+1/2}$ and $W_{i+1/2}$, C and $\varphi_{i+1/2}$ are determined by the boundary conditions for $n(x)$. If we substitute the boundaries $x = x_i$ and $x = x_{i+1}$ we get

$$n_i \equiv n(x_i) = \frac{\varphi_{i+1/2}}{W_{i+1/2}} + C\exp\left(\frac{W_{i+1/2}}{D_{i+1/2}} x_i\right) \tag{2.30}$$

and

$$n_{i+1} \equiv n(x_{i+1}) = \frac{\varphi_{i+1/2}}{W_{i+1/2}} + C\exp\left(\frac{W_{i+1/2}}{D_{i+1/2}} x_{i+1}\right) \tag{2.31}$$

We now eliminate C from these to equations to get an expression for the flux

$$\varphi_{i+1/2} = W_{i+1/2} \frac{n_{i+1} - \exp\left(\frac{W_{i+1/2}}{D_{i+1/2}} \Delta x\right) n_i}{1 - \exp\left(\frac{W_{i+1/2}}{D_{i+1/2}} \Delta x\right)} \equiv A_{i+1/2} n_{i+1} - B_{i+1/2} n_i \tag{2.32}$$

For convenience we defined in each interval the constants $A_{i+1/2}$ and $B_{i+1/2}$. The relation between the fluxes in consecutive intervals is given by the continuity equation

$$\frac{n_i^{k+1} - n_i^k}{\Delta t} + \frac{\varphi_{i+1/2}^{k+1} - \varphi_{i-1/2}^{k+1}}{\Delta x} = S_i^k \tag{2.33}$$

The index k runs over time, with $t^{k+1} = t^k + \Delta t$. S_i^k is the source term at position x_i at time t^k. The diffusion coefficient and the drift velocity used to calculate φ^{k+1} are also taken at time t^k. We now substitute equation (2.32) in equation (2.33) and get

$$\frac{B_{i-1/2}^k}{\Delta x} n_{i-1}^{k+1} + \left(\frac{1}{\Delta t} - \frac{A_{i-1/2}^k + B_{i+1/2}^k}{\Delta x}\right) n_i^{k+1} + \frac{A_{i+1/2}^k}{\Delta x} n_{i+1}^{k+1} = \frac{n_i^k}{\Delta t} + S_i^k \tag{2.34}$$

Since we know all the quantities at the time t^k, this equation just gives a linear relationship between the densities at three consecutive positions after a time step Δt. So we have a system of linear equations of the form

$$a_i n_{i-1} + b_i n_i + c_i n_{i+1} = d_i \tag{2.35}$$

with a_i, b_i, c_i and d_i constants. The coefficients of these equations constitute a tridiagonal matrix. Such systems of equations can be solved very efficiently by a method called Gauss elimination, which is discussed in Appendix A.

The exponential scheme applies to neutral particles (metastables) as well as charged particles. In the case of neutral particles the equations simplify somewhat, because the drift velocity is zero.

2.4 BOUNDARY CONDITIONS FOR THE FLUX

When solving the density, we have to observe boundary conditions. These boundary conditions are not given directly for the density itself, but for the particle flux. They say that every particle arriving at the wall disappears from the discharge, i.e. ions recombine and metastables are de-excited. Expression (2.32) for the flux is valid only within an interval between two grid points x_i. For the flux on the left of x_0 and on the right of x_n we have different expressions [MEU95]

$$\varphi_{-1/2} = -\frac{1}{4} v_{th} n_0 + \alpha W_{1/2} n_0 - \beta \sum_p \gamma_p \varphi_{-1/2,p} \tag{2.36}$$

and

$$\varphi_{n+1/2} = \frac{1}{4} v_{th} n_n + \alpha W_{n-1/2} n_n - \beta \sum_p \gamma_p \varphi_{n+1/2,p} \tag{2.37}$$

The first term in these equations is the thermal flux towards to walls. v_{th} is the classical thermal velocity, and it can be found by applying formula (2.4) to the Boltzmann distribution (B.2)

$$v_{th} = \sqrt{\frac{8kT}{\pi m}} \tag{2.38}$$

with m the particle mass. The second term in the equations (2.36) and (2.37) is the drift flux towards the wall. The constant α is 1 if W is directed towards the wall and 0 otherwise. So this term cancels for $W_{1/2} > 0$ and $W_{n+1/2} < 0$, respectively. The last term takes into account the secondary emission of electrons. $\beta = 1$ if the considered species is the electron and 0 for all other species. The index p runs over the different particle species. γ_p is the secondary emission coefficient and is equal to the average number of electrons emitted by one incident particle of species p.

The expressions (2.36) and (2.37) must be used to obtain the first and the last equation of the set of equations (2.35), i.e. the first and the last row of the tridiagonal matrix of coefficients.

2.5 SOLVING THE ENERGY EQUATION

The energy equation (2.25) can also be solved with the exponential scheme. This can be seen by splitting the equation into two equations

$$\frac{\partial n_\varepsilon}{\partial t}+\frac{\partial}{\partial x}\varphi_\varepsilon = S_\varepsilon \tag{2.39}$$

$$\varphi_\varepsilon = W_\varepsilon n_\varepsilon + D_\varepsilon \frac{\partial n_\varepsilon}{\partial x} \tag{2.40}$$

with

$$n_\varepsilon = n_{\mathrm{e}}\bar{\varepsilon} \tag{2.41}$$

$$W_\varepsilon = \frac{5}{3}W_{\mathrm{e}} \tag{2.42}$$

$$D_\varepsilon = \frac{5}{3}D_{\mathrm{e}} \tag{2.43}$$

$$S_\varepsilon = -e\varphi_{\mathrm{e}}E - \nu_\varepsilon n_\varepsilon \tag{2.44}$$

So the electron energy can be regarded as a particle, with a density, flux and source-term. The boundary conditions for the energy are slightly different from the boundary conditions for particles. The factor 1/4 in the equations (2.36) and (2.37) has to be replaced by a factor 1/3. This can be seen by integrating the energy flux ($\propto v^3$) over the Boltzmann distribution. The electron temperature is determined from the energy density by

$$kT_{\mathrm{e}} = \frac{2}{3}\bar{\varepsilon} = \frac{2n_\varepsilon}{3n_{\mathrm{e}}} \tag{2.45}$$

2.6 CALCULATING THE ELECTRIC FIELD

We do not calculate the electric field directly. Because of the boundary conditions is better to calculate first the electric potential. The electric field is related to the potential by

$$E = -\frac{\partial V}{\partial x} \tag{2.46}$$

If we substitute this into the first Maxwell equation (2.26), we obtain the Poisson equation

$$\frac{\partial^2 V}{\partial x^2} = -\frac{\rho}{\varepsilon_0} = -\frac{\sum_p q_p n_p}{\varepsilon_0} \tag{2.47}$$

for the potential in a charged space.

We can discretize equation (2.47) as follows

$$\frac{\partial^2 V}{\partial x^2} = \frac{\partial}{\partial x}\left(\frac{\partial V}{\partial x}\right) \approx \frac{1}{\Delta x}\left(\left(\frac{V_{i+1} - V_i}{\Delta x}\right) - \left(\frac{V_i - V_{i-1}}{\Delta x}\right)\right) =$$
$$\frac{1}{(\Delta x)^2} V_{i-1} - \frac{2}{(\Delta x)^2} V_i + \frac{1}{(\Delta x)^2} V_{i+1} = \frac{-\sum_p q_p n_{p,i}}{\varepsilon_0} \tag{2.48}$$

the index i refers to a the grid point. This again is a system of linear equations with coefficients forming a tridiagonal matrix, and it can be solved by Gauss elimination. If we know the potential we can calculate the field

$$E_{i+1/2} = \frac{V_{i+1} - V_i}{\Delta x} \tag{2.49}$$

This field is supposed to be constant within every interval.

The boundary conditions for the potential are simply the potentials on the electrodes. These potentials can depend upon the external circuit. In our calculations we always put one electrode to earth, following the convention. The other electrode is in contact with a power supply not directly, but trough some electric components. Suppose we have the small network depicted in Figure 2.3.
The current through circuit is given by

$$I = A\left(\sum_p q_p \varphi_{-1/2,p} + \varepsilon_0 \frac{\partial E_{1/2}}{\partial t}\right) \tag{2.50}$$

A is the surface area of the powered electrode. The first term of the expression in parenthesis is the conduction current density at this electrode. This is just the flux of charge. The second term represents the current due to changes in surface-charge density at the electrode. The surface-charge shields the interior of the electrode from the electric field in the discharge in front of the electrode. Any change in this field results in a change in surface-charge density. The current produced by this effect is equivalent to the displacement current arising in the Maxwell equations.
The total current passes through the resistor and charges the capacitor. This results in a voltage V_{RC} across the external components, which influences the voltage across the discharge

$$V_{\text{discharge}} = V_{\text{applied}} - V_{RC} \tag{2.51}$$

The voltage across the external components is

$$V_{RC}{}^{k} = \frac{I^k \Delta t + C V_{RC}{}^{k-1}}{\Delta t + RC} R \tag{2.52}$$

where the index k indicates the iteration, like before. Implicitly an integration is performed of the charges on the capacitor. In the case that we have only a capacitor ($R = \infty$), equation (2.52) simplifies to

$$V_{RC}{}^{k} = V_{RC}{}^{k-1} + \frac{I^{k}\Delta t}{C} \tag{2.53}$$

and if we have only a resistor ($C = 0$)

$$V_{RC}{}^{k} = I^{k} R \tag{2.54}$$

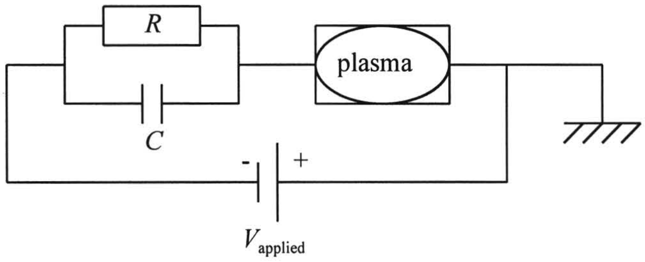

Figure 2.3: External circuit.

2.7 THE TIME STEP AND SPATIAL STEP

The most stringent restriction on the time step arises from the condition that the drift should never be able to reverse the sign of the space-charge [BAR86]. If this would happen, it would lead to instabilities. The condition is

$$\frac{\Delta\rho}{\rho} > -1 \tag{2.55}$$

with $\Delta\rho$ the change in space-charge density in a time step Δt between two iterations. Suppose we have only flux due to drift and no creation or annihilation of particles. For every species p the continuity equation (2.21) reads

$$\begin{aligned} \frac{\partial n_p}{\partial t} &= -\frac{\partial \varphi_p}{\partial x} = -\frac{\partial (W_p n_p)}{\partial x} = -\frac{\partial (s_p \mu_p E n_p)}{\partial x} \\ &= -s_p \mu_p n_p \frac{\partial E}{\partial x} - E \frac{\partial (s_p \mu_p n_p)}{\partial x} \end{aligned} \tag{2.56}$$

We supposed there was only drift, which implies that particle concentration gradients are small, and the last term of equation (2.56) can be neglected. We multiply by q_p, use the first Maxwell equation (2.26), and sum over all the particle species

$$\frac{\partial}{\partial t}\left(\sum_p q_p n_p\right) = -\frac{\rho}{\varepsilon_0}\sum_p q_p s_p \mu_p n_p \tag{2.57}$$

We now discretize this equation and use equation (2.27)

$$\frac{\Delta\rho}{\Delta t} = -\frac{\rho}{\varepsilon_0}\sum_p q_p s_p \mu_p n_p \tag{2.58}$$

Using this expression, we can rewrite condition (2.55) as a restriction on the time step [BAR86] [BOE94]

$$\Delta t \leq \frac{\varepsilon_0}{\sum_p q_p s_p \mu_p n_p} \tag{2.59}$$

The spatial step Δx has also to answer some demands. In cases where the flux due to drift is very high compared to the diffusion flux, a too large Δx can lead to a phenomenon called “numerical diffusion”. A too large Δx can also give rise to “numerical heating” of electrons. One could derive mathematical criteria for Δx, but that is not really necessary. One can easily check if Δx used in a calculation is small enough, by comparing the results with the results of an analogous calculation with a much smaller Δx. If both results are the same, Δx is small enough. For most calculations it is sufficient to take one hundred spatial grid points.

2.8 INPUT DATA FOR THE MODEL

To make calculations with our model, we need to know the electric mobilities, diffusion coefficients, reaction coefficients, and the electron energy loss frequency. In general, these quantities are functions of the electric field or the particle energy. We have two kinds of sources for these data. First, we can find experimentally determined values directly in the literature. Sometimes these data cannot be found. This is especially the case for the quantities concerning electrons. In that case we can use the commercially available Boltzmann solver BOLSIG [BOL96]. This is a computer program that solves the Boltzmann equation (2.1) for electrons in a constant electric field. It is the commercial and user friendly version of the computer code described in [PIT81]. The input of the program consists of cross-sections for many elastic and inelastic collision processes of the electrons with neutral gas particles. These cross-sections as functions of the electron energy are provided with the program for many different gases. The solver finds the electron energy distribution function. By integration it calculates the electron mean energy, i.e. the electron temperature. The electron mobility, electron diffusion coefficient, and the reaction coefficients for ionization and excitation of metastables, are calculated by integrating the cross-sections in question over the electron energy distribution function (see Appendix B). BOLSIG solves the Boltzmann equation for many different electric fields. The output consists of tables of electron temperature, mobility, ionization and excitation coefficients, as functions of the reduced electric field.

Tables of the ion mobility as a function of the reduced electric field for many different ions in many different gases can be found in [ELL76]. The reduced field range covered by these tables is sometimes a bit small. In that case we can extrapolate them to higher values of the reduced field, assuming an reciprocal square-root dependence of the mobility on the field, for it is known that ion drift velocities in high fields increase like the square-root of the field. We can calculate the ion mobility in a mixture by Blanc's law [BLA08]

$$\frac{1}{\mu_p} = \sum_g \frac{f_g}{\mu_{p,g}} \tag{2.60}$$

μ_p is the mobility of ion p in the mixture, $\mu_{p,g}$ is the mobility in gas g, and f_g is the fraction of gas g. Ion free diffusion coefficients cannot be found in the literature, because they cannot be measured directly. In practice one always measures ambipolar diffusion coefficients, and this is not what the model needs. Because the model self-consistently calculates the electric field, the effect of ambipolar diffusion will occur automatically. We therefore have to use the Einstein relation to find the free diffusion coefficient from the mobility

$$D_p = \mu_p \frac{kT_p}{e} \tag{2.61}$$

Notice that this relation agrees with our definitions of the drift velocity (2.14) and the diffusion coefficient (2.15). The ion temperature T_p is usually close to the gas temperature, but in strong electric fields it can become significantly higher. To obtain an estimation of the ion temperature we use a formula given in [ELL76]

$$kT_p = kT + \left(\frac{m_p + m_g}{5m_p + 3m_g} \right) m_g W_p^{\ 2} \tag{2.62}$$

m_p and m_g are the masses of ion p and gas particle g, T is the gas temperature and W_p is the ion drift velocity, which is the product of the ion mobility and the electric field. Metastable species have a mobility equal to zero. Their diffusion coefficients can be found directly in the literature.

For electrons we have the mobility calculated by the Boltzmann solver as a function of the electric field (in local equilibrium, see Section 2.1). What we need is the electron mobility as a function of electron temperature, because we do not make the assumption of local equilibrium for electrons. From the Boltzmann solver we know the electron temperature in local equilibrium

$$T_e = F\left({}^{E}\!/_{p} \right) \tag{2.63}$$

with F a function of E/p. We now make the approximation that the electron distribution function is not affected by a deviation from local equilibrium, but that there is only a “mismatch” between the temperature and the field. We can then define an effective electric field

$$E_{\mathrm{eff}}/p = F^{-1}(T_{\mathrm{e}}) \tag{2.64}$$

which would correspond to our electron temperature in a local equilibrium situation, and use this field to find the electron mobility. For electrons too we use the Einstein relation (2.61) to obtain the free diffusion coefficient.

The source-terms for the particles are calculated from the reaction rate coefficients of the reactions we take into account. In general these coefficients depend on the energy of the reacting particles. Dependence on ion energy is usually not important but the rate coefficients of the reactions involving electrons (especially if they are energy consuming like ionization or excitation) may depend strongly upon the electron energy. For ionization and excitation processes the rate coefficients are calculated by BOLSIG as functions of the reduced electric field. To find the appropriate values we use again the effective field (2.64).

We also have to know the source-term for energy arising in the energy equation. The source-term for energy has the form

$$S_{\varepsilon} = -e\varphi_{\mathrm{e}}E - \nu_{\varepsilon}n_{\varepsilon} \tag{2.44}$$

The first term gives the energy the electrons gain by the electric field per volume per unit time and the second term gives the energy the electrons lose in collisions per unit volume per unit time. We use a trick to determine this last term. From the Boltzmann solver we know the electric field one would need to produce our electron temperature in a local equilibrium situation (2.64). In such a situation the gain by the field equals the loss in collisions. This means that our energy loss is equal to the energy the electron would gain in the effective electric field of equation (2.64).

$$\nu_{\varepsilon}n_{\varepsilon} = -e\varphi_{\mathrm{e,eff}}E_{\mathrm{eff}} \tag{2.65}$$

$\varphi_{\mathrm{e,eff}}$ is the electron flux in the effective field and it is equal to

$$\varphi_{\mathrm{e,eff}} = W_{\mathrm{e,eff}}n_{\mathrm{e}} = \left(-\mu_{\mathrm{e}}E_{\mathrm{eff}}\right)n_{\mathrm{e}} \tag{2.66}$$

(In the BOLSIG calculations there is no diffusion.)

Finally we remark that the secondary emission coefficients of the species we want to take into account are part of the input data of the model. These secondary emission coefficients are specific for a particular electrode material and are in general functions of energy of the incident particles. However, almost no data can be found on these secondary emission coefficients. Therefore we usually give these coefficients guessed constant values.

2.8 Input data for the model

3 SPECIES AND REACTIONS

3.1 KINETIC MODELS

So far we left out of consideration the particle species themselves and the processes among them. We will go into this part of the model in this chapter. Of course the composition of the gas determines which particle species can occur and which reactions may happen in the discharge. We need some theory (based on experimental results) for which species and which processes occur in the gas we want to describe with our model. For the most common gases plenty of these theories can be found in the literature, varying from descriptions of a single reaction mechanism or particle property to complete kinetic models. Even in a straightforward pure gas discharge, the numbers of particle species and reactions can be enormous. The parts played by the different species and reactions depend on the discharge conditions. Under certain conditions only a limited number of species and processes is of importance. In order to limit the calculation times, we need to determine which reactions are really important and which species are really worthwhile considering. The numbers of species and processes must be minimized within the desired accuracy of the results.

Unfortunately, the discharge conditions we use cover a rather broad range. We want to study the discharge as well as the afterglow. During the discharge, creation processes are the most important and losses are mainly due to drift the walls. Because the cathode fall in a micro-discharge is relatively large and of crucial importance, it cannot be neglected and we have to deal with extremely strong electric fields and very high electron energies. In the afterglow the electron temperature decreases to the gas temperature and recombination or de-excitation processes become important. The gas pressure we use is always relatively high. So what we need is a limited model of the gas kinetics, which is valid in high pressure and over a broad range of electron temperatures.

3.2 PURE HELIUM

The most interesting gas for the PALC technology is probably helium. It is relatively cheap and the helium particles are small, so that they cause little harm to the electrodes. The helium gas is very well described in the literature, and many articles can be found on the reaction kinetics of a helium plasma.

A rather extensive kinetic model for the pure helium afterglow is provided in [DEL76]. We will take this article as a starting point and add the reactions of ionization and excitation by electron impact, in order to make the model viable in the discharge regime as well. We will also make some considered simplifications. The reaction coefficients of the reactions are in Table 3.1 (Section 3.4).

The helium atom has two metastable excited states, the He(2 ^3S) and the He(2 ^1S) state. These species can be produced by excitation of helium atoms by energetic electrons

$$\mathrm{He} + e^- \rightarrow \mathrm{He}(2\ ^3S) + e^- \qquad (3.1a)$$

$$\mathrm{He} + e^- \rightarrow \mathrm{He}(2\,^1S) + e^- \qquad (3.1b)$$

The singlet state can be converted to the triplet state

$$\mathrm{He}(2\,^1S) + e^- \rightarrow \mathrm{He}(2\,^3S) + e^- \qquad (3.2)$$

This reaction has a very high rate coefficient, and is probably responsible for the fact that $\mathrm{He}(2\,^3S)$ is usually far more abundant than $\mathrm{He}(2\,^1S)$ [DEL76]. In the afterglow, when almost no excitations take place, $\mathrm{He}(2\,^1S)$ rapidly disappears due to this reaction.
The atomic triplet metastables can be converted in a molecular metastable species $\mathrm{He}_2(2s\,^3\Sigma_u)$ in collisions with two atoms in the ground state

$$\mathrm{He}(2\,^3S) + 2\mathrm{He} \rightarrow \mathrm{He}_2(2s\,^3\Sigma_u) + \mathrm{He} \qquad (3.3)$$

The three metastable states are annihilated by de-excitation processes

$$\mathrm{He}(2\,^3S) + e^- \rightarrow \mathrm{He} + e^- \qquad (3.4a)$$
$$\mathrm{He}(2\,^1S) + \mathrm{He} \rightarrow 2\mathrm{He} \qquad (3.4b)$$
$$\mathrm{He}_2(2s\,^3\Sigma_u) + e^- \rightarrow 2\mathrm{He} + e^- \qquad (3.4c)$$

The atom in the ground state and the atomic metastables can be ionized by electron impact

$$\mathrm{He} + e^- \rightarrow \mathrm{He}^+ + 2e^- \qquad (3.5)$$

$$\mathrm{He}(2\,^3S) + e^- \rightarrow \mathrm{He}^+ + 2e^- \qquad (3.6a)$$
$$\mathrm{He}(2\,^1S) + e^- \rightarrow \mathrm{He}^+ + 2e^- \qquad (3.6b)$$

The electron energy required for the direct ionization of the ground state is much higher than the energy needed for the (stepwise) ionization of the metastables.
The atomic ions can be easily converted into molecular ions in a three body reaction

$$\mathrm{He}^+ + 2\mathrm{He} \rightarrow \mathrm{He}_2^+ + \mathrm{He} \qquad (3.7)$$

These molecular ions can be converted into heavy molecular ions He_3^+, which are also stable at room temperature, by an analogous reaction. However, the reaction rate of this of reaction is unknown and virtually nothing is known about the abundance and reaction kinetics of He_3^+ ions in a high-pressure discharge and afterglow [STE82]. In many experiments they are difficult to distinguish from He_2^+. The best thing to do is to consider the heavy molecular ions as a small additional degeneracy of the He_2^+ state. Bivalent helium ions are not mentioned in [DEL76], nor in any other article on high-pressure helium discharges, and are therefore assumed to play part of importance.

The metastable excitation energies are so high that ions can also be produced in metastable-metastable ionizations. Two metastables of possibly different kinds create either an atomic or a molecular ion in a collision. Each time, the probability of the creation of a molecular ion is 70% [DEL76].

$$\begin{aligned}
&He(2\,^3S) + He(2\,^3S) \rightarrow He^+ + He + e^- && (3.8a)\\
&\qquad\qquad\qquad\qquad \rightarrow He_2^+ + e^- &&\\
&He(2\,^3S) + He(2\,^1S) \rightarrow He^+ + He + e^- && (3.8b)\\
&\qquad\qquad\qquad\qquad \rightarrow He_2^+ + e^- &&\\
&He(2\,^3S) + He_2(2s\,^3\Sigma_u) \rightarrow He^+ + 2He + e^- && (3.8c)\\
&\qquad\qquad\qquad\qquad \rightarrow He_2^+ + He + e^- &&\\
&He(2\,^1S) + He(2\,^1S) \rightarrow He^+ + He + e^- && (3.8d)\\
&\qquad\qquad\qquad\qquad \rightarrow He_2^+ + e^- &&\\
&He(2\,^1S) + He_2(2s\,^3\Sigma_u) \rightarrow He^+ + 2He + e^- && (3.8e)\\
&\qquad\qquad\qquad\qquad \rightarrow He_2^+ + He + e^- &&\\
&He_2(2s\,^3\Sigma_u) + He_2(2s\,^3\Sigma_u) \rightarrow He^+ + 3He + e^- && (3.8f)\\
&\qquad\qquad\qquad\qquad \rightarrow He_2^+ + 2He + e^- &&
\end{aligned}$$

The atomic ions perish due to radiative recombination and three-body recombination

$$\begin{aligned}
&He^+ + e^- \rightarrow He + h\nu && (3.9)\\
&He^+ + 2e^- \rightarrow He + e^- && (3.10)
\end{aligned}$$

Molecular ions are lost in a two-body recombination process. This either results in atomic triplet metastable states or in ground state helium atoms

$$\begin{aligned}
&He_2^+ + e^- \rightarrow He(2\,^3S) + He && (3.11)\\
&\qquad\qquad \rightarrow 2He &&
\end{aligned}$$

The branch ratios of these two reaction branches are 5/9 and 4/9, respectively [STE82].

It turns out that all metastable species participate in similar reactions, with similar reaction rate coefficients. Moreover, the diffusion coefficients of the different metastables are approximately the same. Therefore, it is possible to combine the three metastable species into one "general" metastable. This considerably reduces the numbers of reactions and species. The excitation reactions (1a) and (1b) become one reaction for the excitation of the general metastable (we will indicate it by He^*). The excitation coefficient for He^* is equal to the sum of the excitation coefficients for $He(2\,^3S)$ and $He(2\,^1S)$. The metastable conversion reactions (3.2) and (3.3) disappear. The metastable de-excitation reactions (3.4) give a small problem. Reactions (3.4a) and (3.4c) are analogous and have the same rate coefficient, but reaction (3.4b) is different and in almost all circumstances slower than (3.4a) and (3.4c). We assume here that the de-excitation of He^* has the reaction rate of the reactions (3.4a) and (3.4c). By doing this, we overestimate the true de-excitation rate. This is not really a problem all the same; the approximation is better as the share of the $He(2\,^1S)$ metastables is smaller and there is experimental evidence that in the afterglow by far the most important metastable species is $He(2\,^3S)$ [STE81] [DEL76]. Moreover, during the discharge, when the metastable densities are high, the de-excitation is negligible as a loss process for metastables compared to metastable-metastable ionization.

Another critical point in the approximation of taking all metastables together, is the stepwise ionization. The ionization coefficient is the same for both atomic metastables, but the molecular metastable is not liable to ionization at all, at least none of the articles found mentioned such a thing. Nevertheless we assume that the coefficient for ionization of He^* is the same as that of reactions (3.6), which could mean an overestimation. However, it can be shown that the molecular metastable density during a discharge is small compared to the atomic metastable density. The molecular metastables are produced in reaction (3.3) with a rate of 0.23×10^{-33} $[He(2\,^3S)][He]^2$ $cm^{-3}s^{-1}$. One of the loss processes is reaction (3.8f), which has a reaction rate of 2.5×10^{-9} $[He_2(2s\,^3\Sigma_u)]^2$ $cm^{-3}s^{-1}$. Comparing these two rates at a pressure of 200 Torr gives $[He_2(2s\,^3\Sigma_u)] < 10^4\,[He(2\,^3S)]^{1/2}$, which means that $[He_2(2s\,^3\Sigma_u)] << [He(2\,^3S)]$ if $[He(2\,^3S)] >> 10^8$ cm^{-3}.
The reaction coefficients for all of the metastable-metastable ionization reactions are the same, regardless of which metastables participate in the reaction. This means that the reactions (3.8a)-(3.8f) can be replaced without any trouble by one reaction for ionization by two He^* particles.
We end with the following set of reactions

$$He + e^- \rightarrow He^* + e^- \tag{3.1}$$
$$He^* + e^- \rightarrow He + e^- \tag{3.4}$$
$$He + e^- \rightarrow He^+ + 2e^- \tag{3.5}$$
$$He^* + e^- \rightarrow He^+ + 2e^- \tag{3.6}$$
$$He^+ + 2He \rightarrow He_2^+ + He \tag{3.7}$$
$$\begin{aligned} He^* + He^* &\rightarrow He^+ + He + e^- \\ &\rightarrow He_2^+ + e^- \end{aligned} \tag{3.8}$$
$$He^+ + e^- \rightarrow He + h\nu \tag{3.9}$$
$$He^+ + 2e^- \rightarrow He + e^- \tag{3.10}$$
$$\begin{aligned} He_2^+ + e^- &\rightarrow He^* + He \\ &\rightarrow 2He \end{aligned} \tag{3.11}$$

3.3 HELIUM-NITROGEN MIXTURES

Although helium has many excellent properties, an afterglow in pure helium may last too long for PALC applications. It turns out that the helium metastables are responsible for this slow decay [ILC96]. One way to solve this problem is to add a small percentage of neon or xenon. The ionization energy in these gases is lower than the excitation energy of the helium metastable states. Consequently the helium metastables are able to ionize neon or xenon atoms. These processes are called Penning ionizations and they provide an effective annihilation channel for helium metastables, thus shortening the afterglow. However, neon or xenon appear to be inappropriate for PALC because they cause sputtering of the electrode material. Another (less known) Penning mixture is that of helium and (a small percentage of) nitrogen. Nitrogen seems to cause no sputtering and might therefore be useful in PALC. This is the reason that we study helium-nitrogen mixtures here.

Although the literature on these mixtures is not very extensive, enough information about them can be found to put together a viable kinetic model. The most complete description of the processes in helium-nitrogen mixtures is given by [POU82]. Like [DEL76], this article concentrates on the afterglow, so that no excitations or ionizations by electron impact are included. The reactions and species considered in [POU82] agree nicely with the reactions in pure helium that we ended with in the preceding section. We stick to these reactions and add the reactions in which nitrogen particles are involved. In [POU82] there is discriminated between molecular nitrogen ions in different metastable excited states. We will not use this distinction because all the ionic metastables react in exactly the same way, and can be regarded as one species without any further assumption. In [POU82] the distinction is merely drawn because they use their model to explain optical measurements of transitions between the ionic metastable states. So we consider only one species of molecular nitrogen ions. They are created from nitrogen molecules by electronic ionization

$$N_2 + e^- \rightarrow N_2^+ + 2e^- \qquad (3.12)$$

Nitrogen ions do also arise from charge exchange reactions, in which a helium ion takes an electron from a nitrogen molecule. These processes can occur because the ionization energy of helium is higher than that of nitrogen. The released energy can be used to dissociate the molecular nitrogen ion in an atomic nitrogen ion and a radical nitrogen atom. The chance for this dissociation to occur is 50% [POU82].

$$\begin{aligned} He^+ + N_2 &\rightarrow N_2^+ + He \\ &\rightarrow N^+ + N + He \end{aligned} \qquad (3.13)$$

This reaction has a three-body version

$$\begin{aligned} He^+ + N_2 + He &\rightarrow N_2^+ + 2He \\ &\rightarrow N^+ + N + 2He \end{aligned} \qquad (3.14)$$

These charge exchange reactions do also arise with molecular helium ions. In this case dissociation has a probability of 75% [POU82].

$$\begin{aligned} He_2^+ + N_2 &\rightarrow N_2^+ + 2He \\ &\rightarrow N^+ + N + 2He \end{aligned} \qquad (3.15)$$

$$\begin{aligned} He_2^+ + N_2 + He &\rightarrow N_2^+ + 3He \\ &\rightarrow N^+ + N + 3He \end{aligned} \qquad (3.16)$$

A third way in which nitrogen ions are produced is by the Penning process mentioned before. The helium metastable is de-excited on ionizing a nitrogen molecule

$$He^* + N_2 \rightarrow N_2^+ + e^- + He \qquad (3.17)$$

This reaction too has a three-body counterpart

$$He^* + N_2 + He \rightarrow N_2^+ + e^- + 2He \qquad (3.18)$$

The single nitrogen atoms, which are produced in the dissociation of molecular nitrogen ions, are also subject to Penning reactions

$$He^* + N \rightarrow N^+ + e^- + He \tag{3.19}$$

The molecular and atomic nitrogen ions are destroyed in recombination processes

$$N_2^+ + e^- \rightarrow 2N \tag{3.20}$$
$$N^+ + e^- \rightarrow N + h\nu \tag{3.21}$$

The atomic nitrogen too disappears by recombination

$$N + N + He \rightarrow N_2 + He \tag{3.22}$$

3.4 DATA

In the previous two sections it turned out that for the modeling of helium nitrogen mixtures we have to take into account 9 particle species, viz.

- electrons
- helium gas atoms, He
- atomic helium ions, He^+
- molecular helium ions, He_2^+
- general helium metastables, He^*, the properties of which look most like those of the $He(2\,^3S)$ excited state
- nitrogen gas molecules, N_2
- atomic nitrogen ions, N^+
- molecular nitrogen ions, N_2^+
- radical single nitrogen atoms, N

(In pure helium we have only the first 5 species.) We assume that the densities of helium gas atoms and nitrogen gas molecules are several orders of magnitude bigger than the densities of the other species, so that they are not affected by the reaction kinetics. Of the remaining 7 species we need to know several properties, as we pointed out in Section 2.8. Furthermore we need to known the rate coefficients of the reactions (3.1) and (3.4)-(3.22). All these data will be presented in this section. The properties of the particles and the reaction coefficients may depend on the percentage of nitrogen in a helium nitrogen mixture. We will confine ourselves to 4 different percentages of nitrogen viz. 0%, 0.1%, 0.2%, and 0.5%.

The electron temperature as a function of the reduced electric field is depicted in Figures 3.1 and 3.2. The data for $E/p > 1$ are obtained by calculation with a Boltzmann solver (see Section 2.8). The values for $E/p < 1$ (Figure 3.2) come from a calculation by L.S. Frost and A.V. Phelps and are published on page 536 of [MCD64]; they agree with lots of experiments. In the low field limit the electron temperature approaches the gas temperature. (300 K corresponds to a particle mean energy of 0.039 eV)

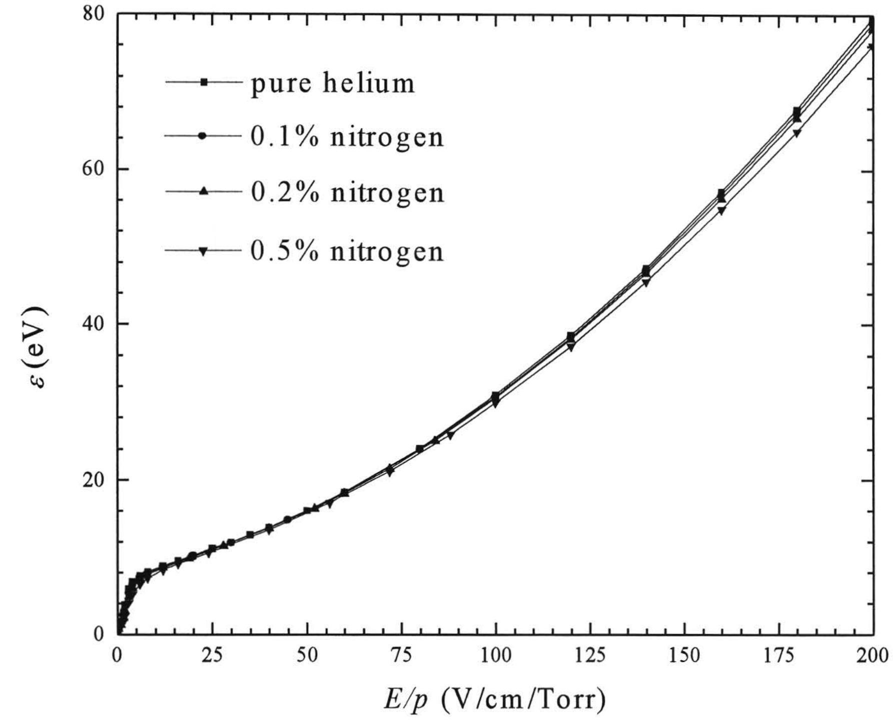

Figure 3.1: Electron temperature in helium-nitrogen mixtures as a function of *E/p* for different percentages of nitrogen. The curves are calculated by BOLSIG.

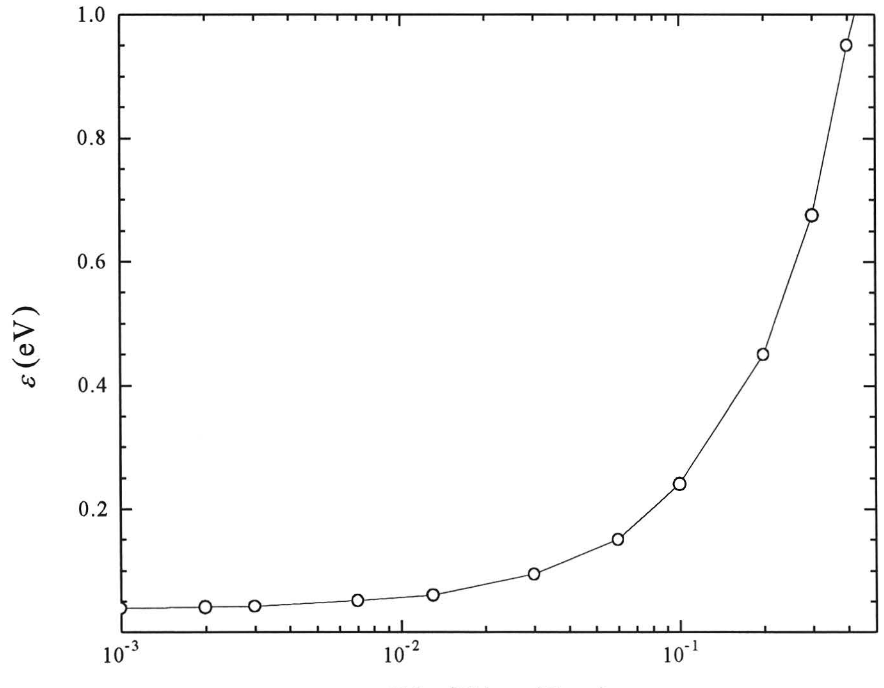

Figure 3.2:Electron temperature in pure helium as a function of *E/p*. The data are taken from [MCD64]

The electron mobility is displayed in Figure 3.3. (We plotted only the values for pure helium, because there was no visible difference in the electron mobility for the different

Boltzmann solver and the data for *E/p* < 1 are taken from [MCD64]. The latter values are based on measurements of drift velocities. It turns out that in very small electric fields (*E/p* << 1) the electron mobility is about one order of magnitude bigger than for *E/p* > 1. This comes from a decline in the elastic collision cross-section for very small electron energy due to so-called Ramsauer effects (quantum mechanical effects). If we calculate the electron diffusion coefficient at room temperature by applying the Einstein relation (2.61) to the low field limit of the electron mobility ($8.3\text{x}10^6$ cm^2/Vs), we obtain a value of $2.2\text{x}10^5$ cm^2/s. This agrees with measured values for the diffusion coefficient of thermalized electrons in pure helium [RAI91] [HAS72].

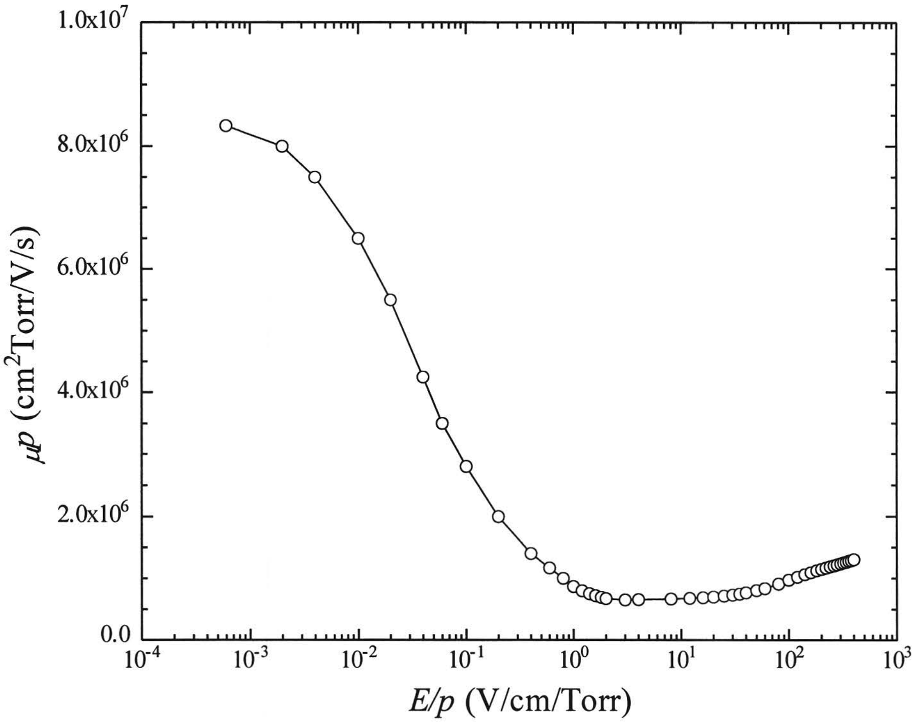

Figure 3.3: Electron mobility in pure helium as a function of *E/p*. The data come from [MAC61] and a BOLSIG calculation.

The mobilities of the four ion species in pure helium are shown in Figure 3.4. The ion mobilities in the helium nitrogen mixtures can be calculated from these data and from analogous data for the mobilities in pure nitrogen by Blanc's law (2.60). For the small percentages of nitrogen we use they are almost the same as the mobilities in pure helium; the difference is at most a few percents. The data are taken from [ELL76] and [MCF73], and possibly extended to higher fields by extrapolation as the reciprocal square root of *E/p*. The range of *E/p* covered by the data on the mobility of N^+ is so small that it is impossible to make the extrapolation in a proper way. We therefore assume that the mobility of N^+ in high fields is constant, being aware of the fact that this assumption could be even more mistaken than an extrapolation as the reciprocal square root of *E/p* . Notice that the mobility of atomic helium ions is about half as small as the mobilities of the other ions. The reason for this is that atomic helium ions, unlike the other ions, are subject to charge transfer reactions with helium gas atoms.

These reactions constitute an effective loss mechanism for ion momentum, thus increasing the ion momentum transfer frequency and limiting the ion mobility.

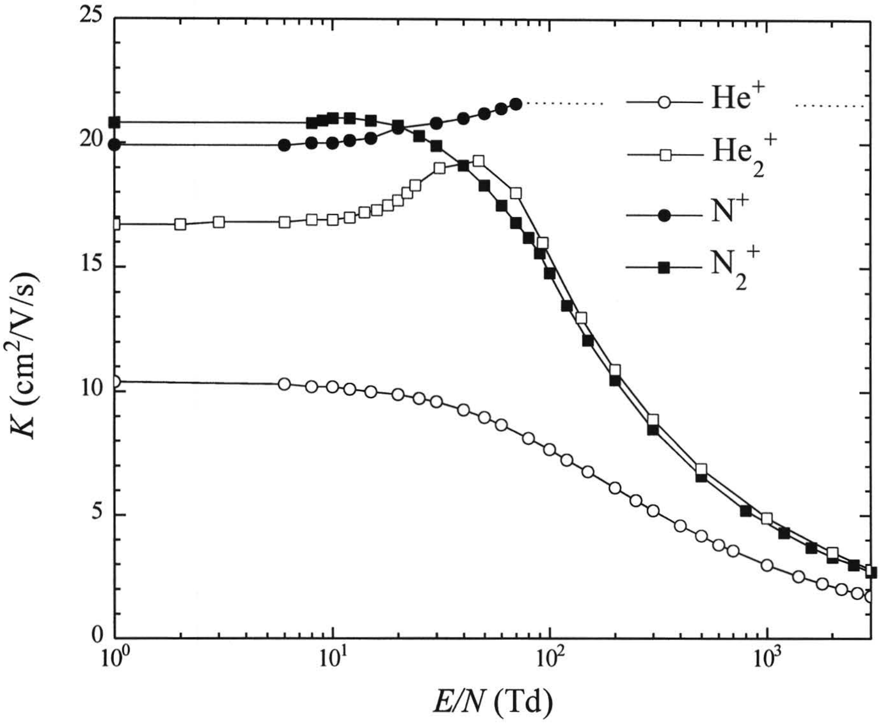

Figure 3.4: The reduced mobilities K of the different ions in helium as a function of E/N. The data are taken from [ELL76] and [MCF73]. The reduced mobility is defined as $K = \mu \cdot (p/760) \cdot (273.15/T)$, with p and T neutral gas pressure and temperature in Torr and K, respectively. An E/N value of 1 Td corresponds to an E/p value of 0.33 V/cm/Torr.

For the diffusion coefficient at room temperature of the general metastable He* in pure helium we take $D \cdot p = 420$ cm^{2}Torr/s, following [CHA92]. According to [MON70] the diffusion coefficient of single nitrogen atoms N in helium is equal to $D \cdot p = 133$ cm^{2}Torr/s. We assume that these values apply also to the helium nitrogen mixtures we use.

The rate coefficients of the reactions we take into account are given in Table 3.1. Some coefficients are taken constant and others are given as functions of the electron mean energy or the reduced electric field. The latter are shown in Figures 3.6-3.9.

Table 3.1: Reaction rate coefficients. Some reaction coefficients are constant and some are read from lookup-tables.

Reaction	Rate coefficient		Source
(3.1)	Table, see Figure 3.6	(3.1a)+(3.1b)	Boltzmann solver
(3.1a)	Table, see Figure 3.5		Boltzmann solver
(3.1b)	Table, see Figure 3.5		Boltzmann solver
(3.2)	1.5×10^{-7} cm^{3}s^{-1}		[DEL76]
(3.3)	0.23 Torr^{-1}s^{-1}		[DEL76]
(3.4)	2.9×10^{-9} cm^{3}s^{-1}	(3.4a)	[STE82]
(3.4a)	2.9×10^{-9} cm^{3}s^{-1}		[STE82]
(3.4b)	142.8 Torr^{-1}s^{-1}		[DEL76]
(3.4c)	2.9×10^{-9} cm^{3}s^{-1}		[STE82]
(3.5)	Table, see Figure 3.7		Boltzmann solver
(3.6)	Table, see Figure 3.8	(6a)=(6b)	[JAN87]
(3.6a)	Table, see Figure 3.8		[JAN87]
(3.6b)	Table		[JAN87]
(3.7)	1.5×10^{-31} cm^{6}s^{-1}		[POU82]
(3.8)	2.9×10^{-9} cm^{3}s^{-1}		[STE82]
(3.8a)-(3.8f)	1.5×10^{-9} cm^{3}s^{-1}		[DEL76]
(3.9)	$4.2\times10^{-12}(T_e/300)^{-0.5}$ cm^{3}s^{-1}	(outdated, [STE82])	[CHA92]
(3.10)	$6.0\times10^{-20}(T_e/300)^{-4.0}$ cm^{6}s^{-1}		[CHA92]
(3.11)	9×10^{-9} cm^{3}s^{-1}		[STE82]
(3.12)	Table, see Figure 3.9		Boltzmann solver
(3.13)	1.2×10^{-9} cm^{3}s^{-1}		[POU82]
(3.14)	2.2×10^{-29} cm^{6}s^{-1}		[POU82]
(3.15)	1.1×10^{-9} cm^{3}s^{-1}		[POU82]
(3.16)	1.36×10^{-29} cm^{6}s^{-1}		[POU82]
(3.17)	7.6×10^{-11} cm^{3}s^{-1}		[POU82]
(3.18)	3.3×10^{-30} cm^{6}s^{-1}		[POU82]
(3.19)	1.6×10^{-10} cm^{3}s^{-1}		[POU82]
(3.20)	1.0×10^{-7} cm^{3}s^{-1}		[POU82]
(3.21)	5×10^{-9} cm^{3}s^{-1}		[POU82]
(3.22)	1.15×10^{-29} cm^{6}s^{-1}		[POU82]

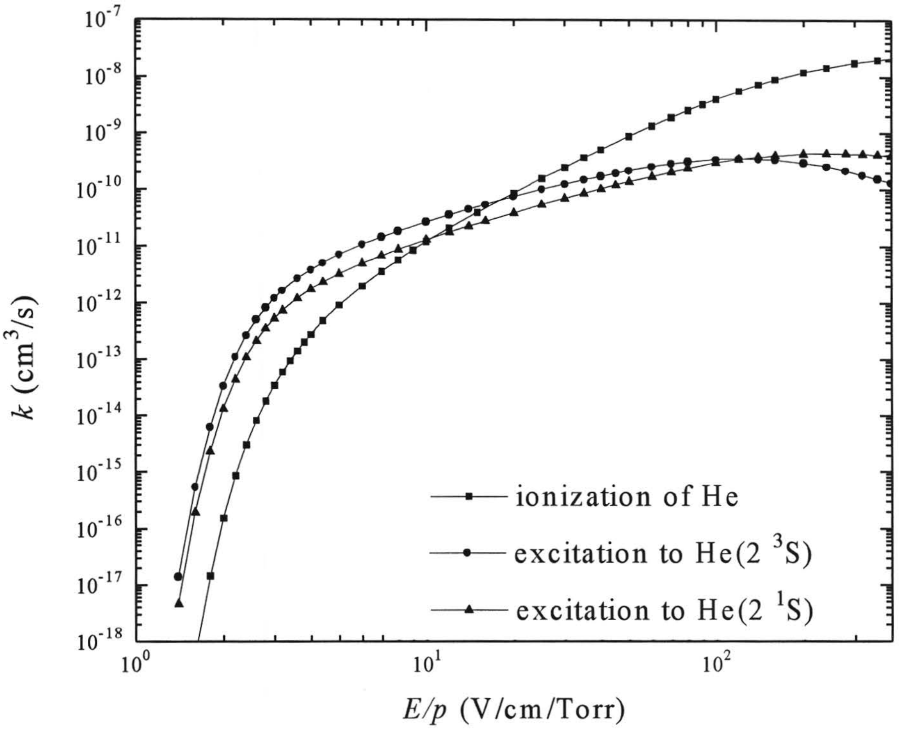

Figure 3.5: The reaction rate coefficients for the excitation of helium to the 2^3 S state (3.1a), the 2^1 S state (3.1b) and the ionization of helium (3.5), as functions of *E/p*. All data are calculated from cross-sections by BOLSIG.

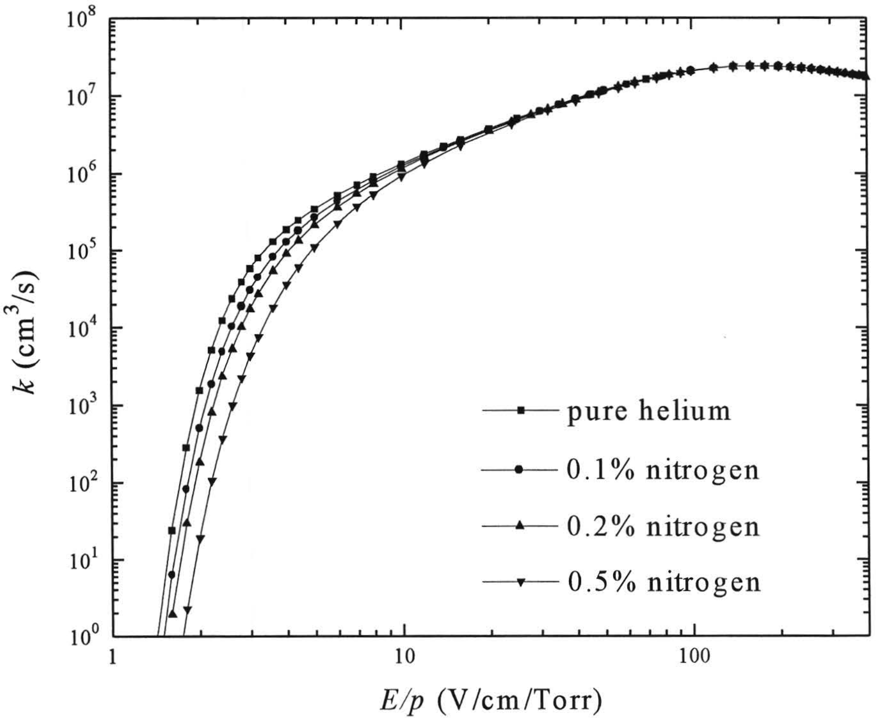

Figure 3.6: The reaction rate coefficient for the excitation of helium (3.1) as a function of *E/p*; calculated by BOLSIG for different percentages of nitrogen.

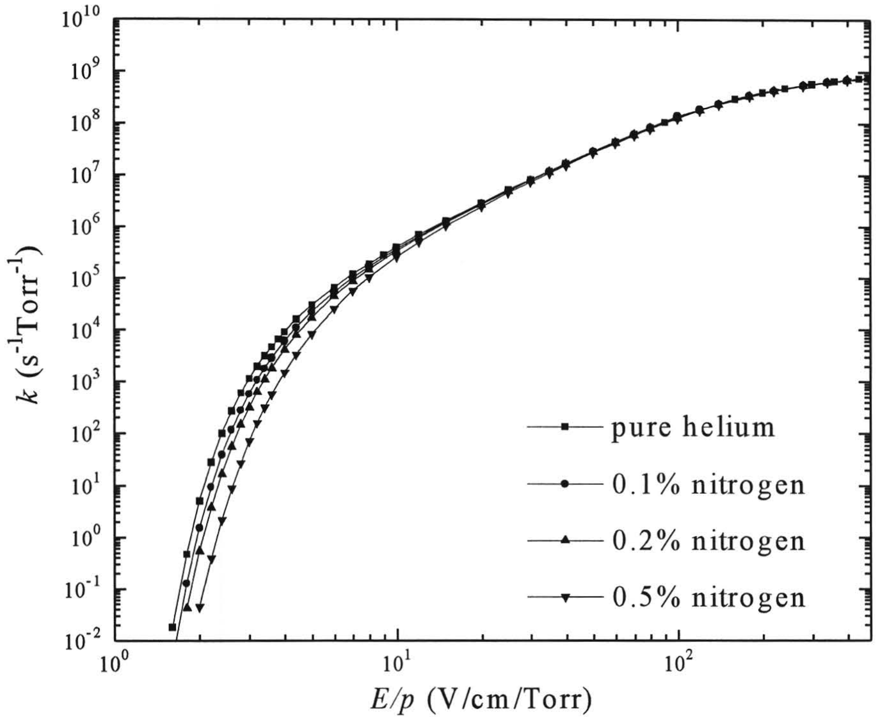

Figure 3.7: The reaction rate coefficient for the ionization of helium (3.5) as a function of *E/p*; calculated by BOLSIG for different percentages of nitrogen.

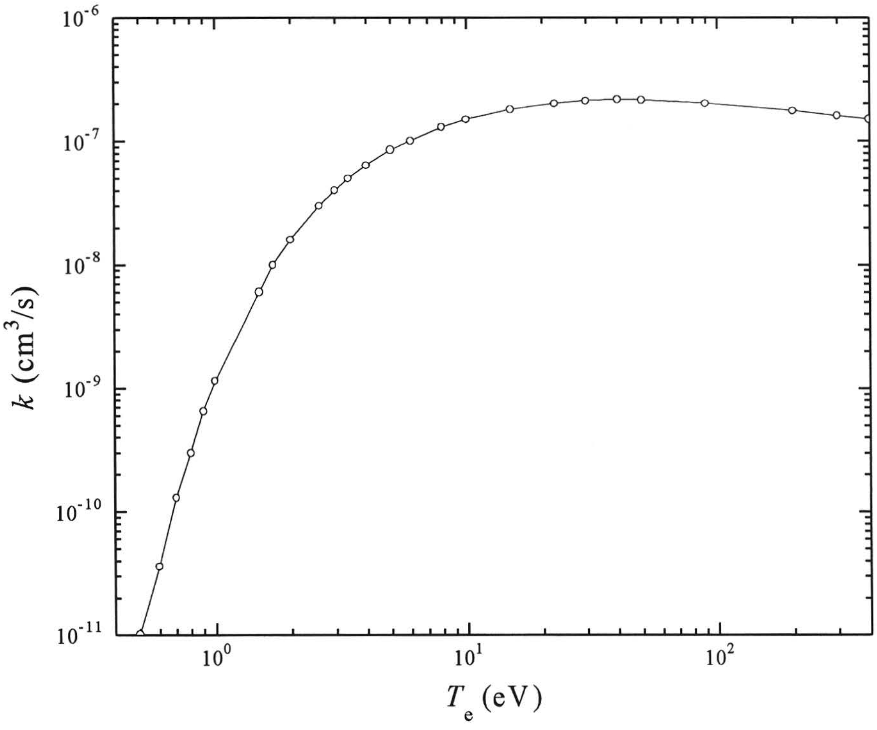

Figure 3.8: The reaction rate coefficient for the ionization of He(2^3 S) (3.6a) as a function of the electron temperature. The data are taken from [JAN87].

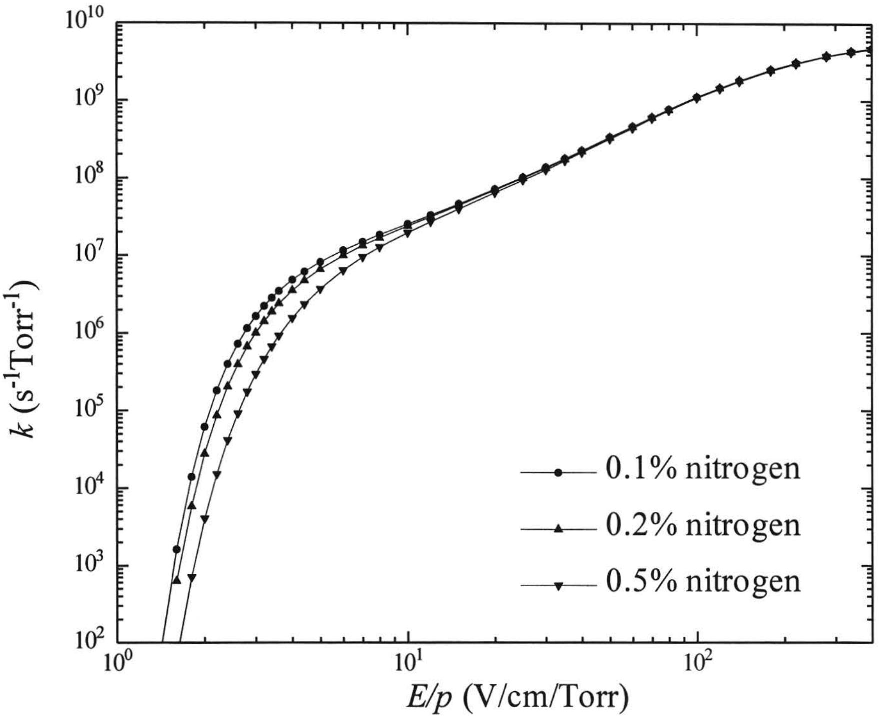

Figure 3.9: The reaction rate coefficient for the ionization of nitrogen (3.12) as a function of *E*/*p*; calculated by BOLSIG for different percentages of nitrogen. This coefficient is given per unit of partial nitrogen pressure (and not per unit of total gas pressure)

3.4 Data

4 RESULTS AND CONCLUSIONS

4.1 A DC DISCHARGE IN PURE HELIUM

In this chapter we will use the model discussed in the preceding chapters to do computer simulations that tell us something about PALC. We implement our model into a Borland C++ computer code. The resulting program runs on a PC with a Pentium 133 processor sufficiently fast so as to keep the calculation times within reasonable limits (several hours). Let us first consider the PALC configuration. Figure 4.1 displays a cross-section through a PALC panel perpendicular to the discharge channels.

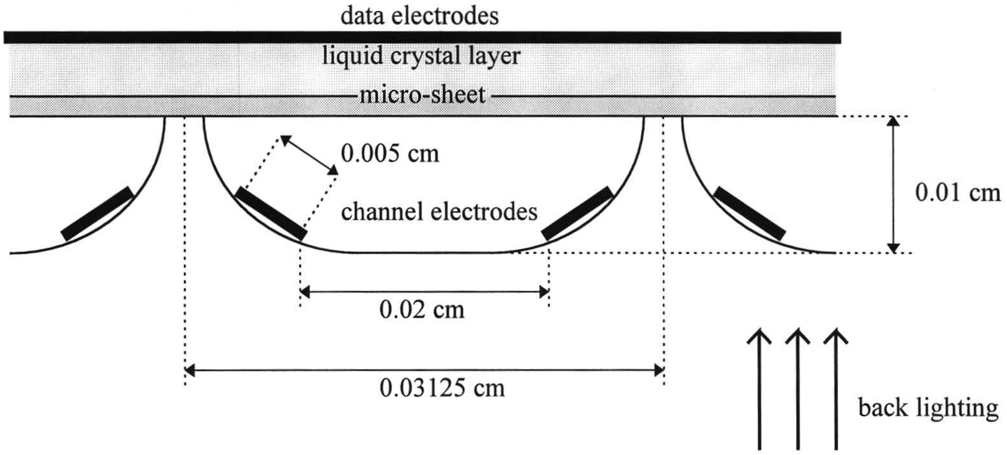

Figure 4.1: Cross-section through a PALC panel perpendicular to the discharge channels. Typical distances are indicated. The liquid crystal layer is protected from the plasma in the channel by a thin micro-sheet.

Unfortunately we cannot give an exact simulation of a PALC channel because 1) the model is only one dimensional while a realistic description of a PALC channel needs to take into account at least two spatial dimensions and 2) it is impossible to simulate the breakthrough of the discharge. What we can do however, is simulate a fully developed DC glow discharge between two parallel flat plate electrodes (see Section 1.4) at a very small distance. This gives us an idea about the densities of the different species at the end of a discharge pulse.

First, we will simulate the steady state of a DC discharge in pure helium. For the distance between the electrodes we take 0.025 cm. This is approximately the same as the distance between the channel electrodes (see Figure 4.1). The gas pressure is put to 200 Torr, which is a typical pressure for PALC discharges. The secondary emission coefficients are assumed to be 0.1 for all ions and metastables. We apply a voltage of 350 Volts directly to the electrodes, which is again a typical value. We start with sine-shaped density profiles with a maximum of 1×10^{10} cm^{-3} midway between the electrodes. After several hours of calculation time and several microseconds of calculated time the densities reach a steady state.

The density profiles in this steady state are displayed in Figure 4.2. The cathode is in the left-hand side of this figure. In front of this cathode there is the cathode fall region in which practically no electrons are present. This cathode fall extends to approximately halfway the electrodes. The most important ion in the cathode fall is He^+. In the plasma both ions He^+ and He_2^+ are of about equal importance. By far the most abundant species is the helium metastable. Because these metastable atoms are neutral, they are not subject to drift or ambipolar diffusion and can accumulate to really high concentrations.

The reduced electric field and the electron mean energy are depicted in Figure 4.3 as functions of the position. The electric field is almost zero in the plasma and in the cathode fall it depends approximately linearly on the distance to cathode. The electron energy is about 6 eV in the plasma and reaches the extremely high value of 45 eV in the cathode fall. This figure demonstrates clearly that it is necessary to include the energy equation for electrons in the model, for there is no direct and monotonous relationship between the reduced electric field and the electron energy. The secondary electrons are emitted with a low energy into the very high electric field in front of the cathode. Figure 4.3 shows that they do not attain a thermal equilibrium immediately, but need a non negligible traveling distance to pick up energy from the field. (Their energy increases while the field decreases.) Figure 4.3 also displays the electron energy due to directed motion $1/2\ m_e(\varphi_e/n_e)^2$. In the derivation of our equations we assumed that this gives only a negligible contribution to the mean electron energy (2.11). Figure 4.3 shows that in the plasma this assumption is absolutely justified, but in the cathode fall the result is less convincing. Although in this case the requirement (2.11) is reasonably well met in the cathode fall, we want to point out that one has to be careful.

The reaction rate profiles are depicted in Figures 4.4 and 4.5. Figure 4.4 shows the creation and conversion processes. The excitation and ionization processes occur mainly at border of the cathode fall, where both the electron energy and the electron density are high. As the threshold energy of the process is higher, the influence of the electron energy is bigger and the maximum in the reaction rate is located more towards the cathode. Notice that the density profile of metastables (see Figure 4.2) looks much like the excitation rate profile. Figure 4.5 displays the annihilation reaction rates. These reactions rates turn out to be at least two orders of magnitude smaller than the rates for the creation processes. This means that almost all particles are lost by drift and diffusion towards the electrodes.

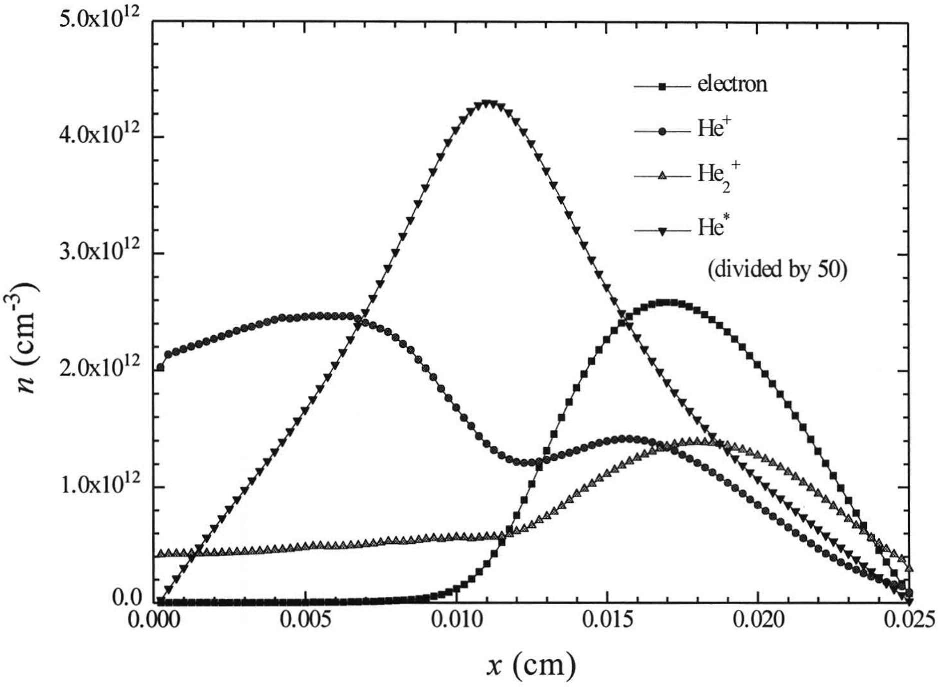

Figure 4.2: Density profiles of the different species in a DC discharge in pure helium. The gas pressure is 200 Torr, the secondary emission coefficient of all heavy particles is 0.1, and the voltage across the electrodes is 350 V. The cathode is located at $x = 0$ and the anode at $x = 0.025$ cm. Notice that the density of metastables is divided by 50 in order to obtain the same order of magnitude as the densities of the other species.

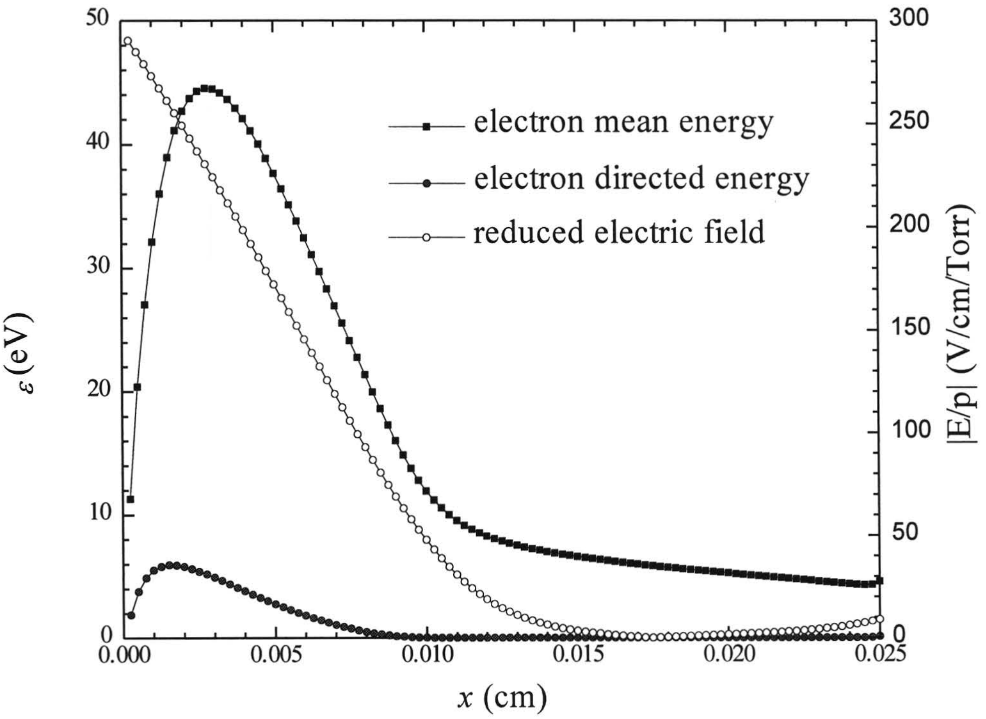

Figure 4.3: The electron mean energy and the electron energy due to systematic motion (scale left), and the reduced electric field (scale right). These curves concern the same simulation as the curves in Figure 4.2.

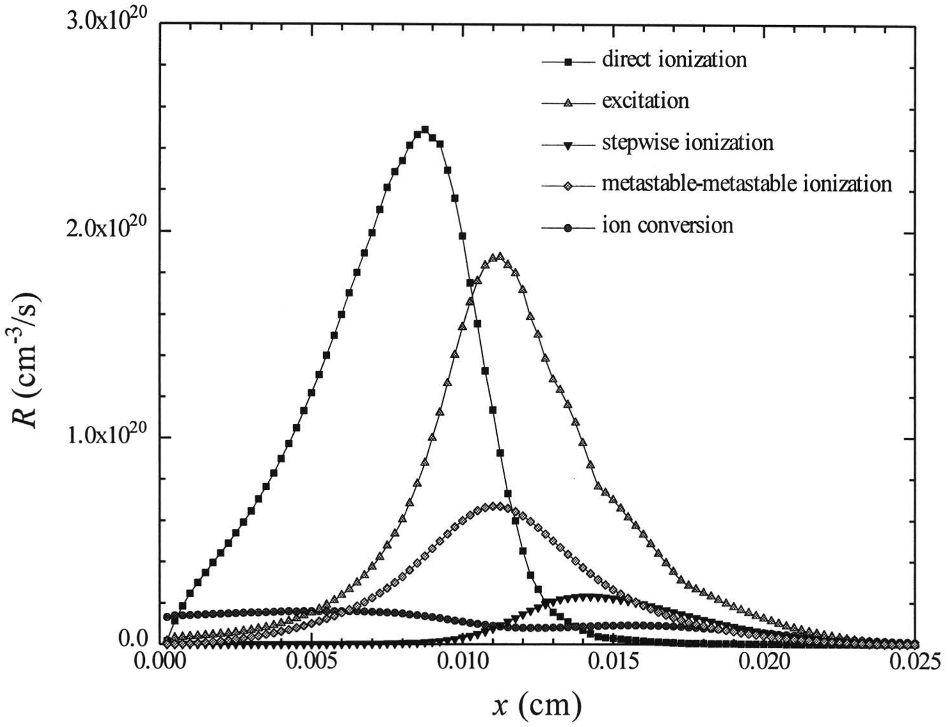

Figure 4.4: Reaction rates for the direct electronic ionization of helium atoms in the ground state (3.5), the excitation to the metastable He(2 S) states (3.1), the electronic ionization of this metastable state (3.6), the metastable-metastable ionization (3.8), and the conversion of atomic ions into molecular ions (3.7). These curves concern the same simulation as the curves in Figure 4.2.

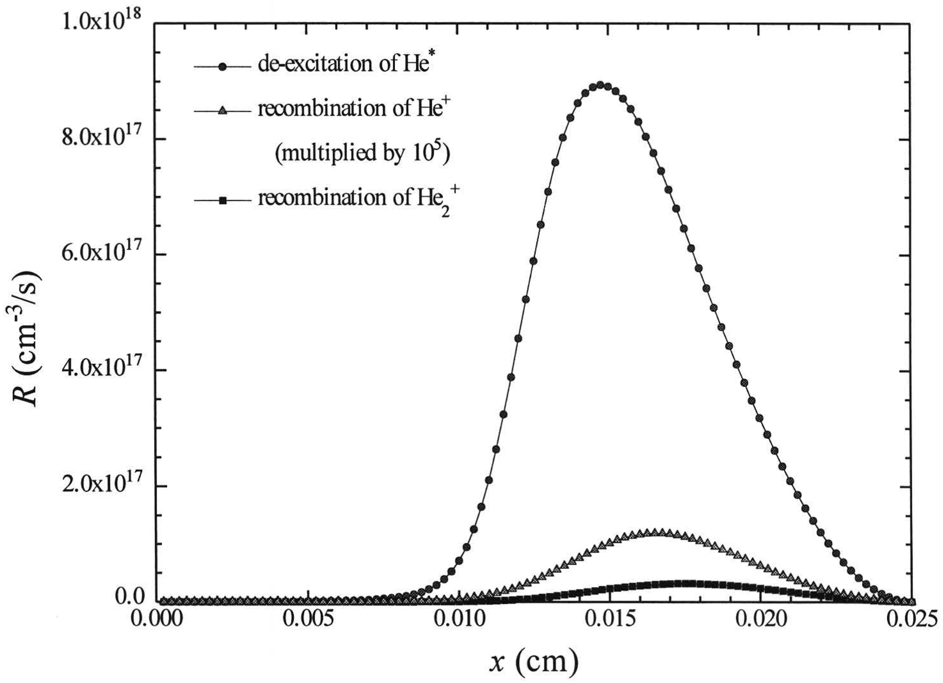

Figure 4.5: Reaction rates for the de-excitation of metastables (3.4), recombination of atomic ions (3.9)+(3.10), and recombination of molecular ions (3.11). Notice that the reaction rate for the recombination of atomic ions is five orders of magnitude smaller than the other rates. These curves concern the same simulation as the curves in Figure 4.2.

An important mistake we make in using this one dimensional simulation for a PALC channel, is that we do not take into account diffusional losses to the top and the bottom of the channel. We will now make a rough estimation of these losses. Imagine we would stop all source terms at once. The densities would start to decay exponentially (see Section 1.5) due to diffusion with a characteristic time τ. The characteristic decay time τ for diffusion in the bottom-to-top direction is given by equation (1.19) with $L = 0.01$ cm (= the height of a PALC channel). For the ambipolar diffusion coefficient we use a value of 200 cm^2/s, which is the average of the ambipolar diffusion coefficients of He^+ and He_2^+ at an electron temperature of 4 eV (this is the electron temperature in the plasma, see Figure 4.3). Equation (1.19) gives $\tau = 5x10^{-8}$ s. The total source term needed to compensate for the diffusional losses is equal to the plasma density divided by this time, $S = n/\tau = 2.5x10^{12}/5x10^{-8} = 5x10^{19}$ cm^{-3}/s in the middle of the plasma. If we compare this rate to the reaction rates in Figures 4.4 and 4.5, we see that it is of the same order of magnitude, which means that the diffusion to the bottom and the top of the channel is certainly not negligible, but is also not dominant. Anyway, to take into account these losses in a proper way requires a two dimensional model.

4.2 INFLUENCES OF PARAMETERS

We will now examine the influence of the pressure on the structure of the one dimensional DC discharge, by doing a number of simulations with various pressures. Every time the electrode distance is 0.025 cm, the secondary emission coefficients are 0.1, and the voltage across the discharge is 350 V. The gas pressures we use are in the range from 150 to 450 Torr. Figure 4.6 displays the densities of electrons and ions for different pressures.

It turns out that the size of the cathode fall decreases as the pressure increases, as we expected from our considerations in Section 1.4. According to the classical scaling law (1.11) the size of the cathode fall is inversely proportional to the gas pressure. In order to verify this law, we will define the boundary of the cathode fall as the point where the electron density is half the ion density. Figure 4.7 shows the size of the cathode fall as a function of the reciprocal pressure. The relationship is approximately linear, in accordance with the scaling law. The offset in d arises from our (somewhat arbitrary) definition of this quantity.

Figure 4.6 shows us also that the plasma density increases with increasing pressure. This effect is illustrated more clearly by Figure 4.8, in which for every species the maximum density is depicted as a function of the gas pressure. It turns out that the contribution of the molecular ions He_2^+ increases with increasing pressure. The reason for this is that the rate of the reaction for the conversion of atomic ions into molecular ions (3.7) is directly proportional to the square of the gas pressure, thus increasing more strongly with increasing pressure than the other reaction rates.

Figure 4.9 illustrates the effect of the gas pressure on the electron energy. As the gas pressure increases, the electric field in the cathode fall is stronger so that the secondary electrons gain energy faster. Moreover, the electrons lose their energy faster upon entering the plasma. The electron temperature in the plasma decreases with increasing pressure. Notice that for relatively high pressure the electrons gain energy again in front of the anode. This arises from a small sheath that is present in front of the anode in high pressures. The occurrence of this so-called anode fall can also be seen in Figure 4.6.

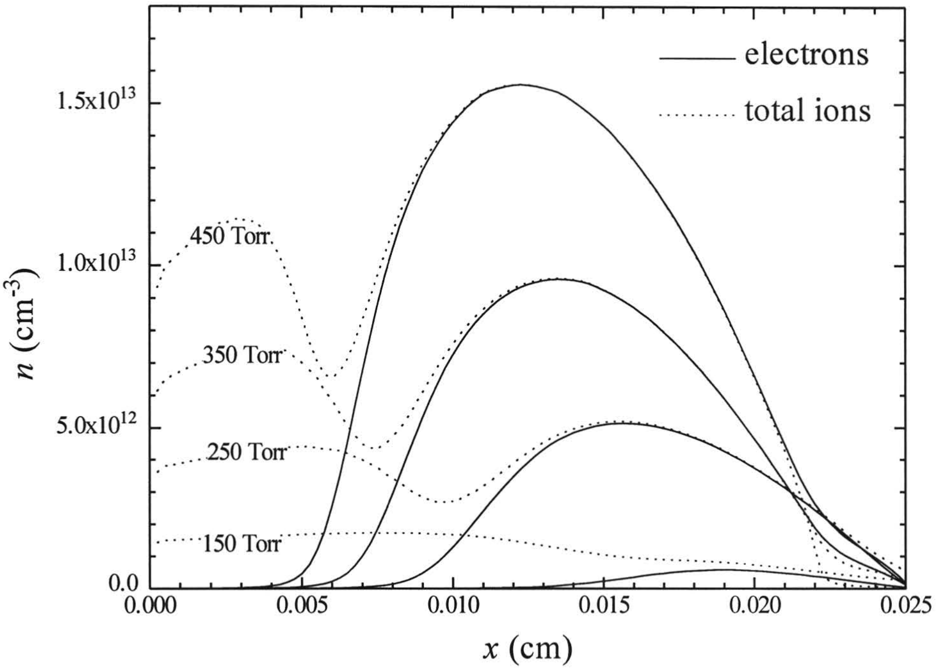

Figure 4.6: The density of electrons and the total density of ions as a function of position for different gas pressures. The DC voltage across the electrodes is every time 350 V; the cathode is located on the left. The secondary emission coefficient is put to 0.1 for all heavy species.

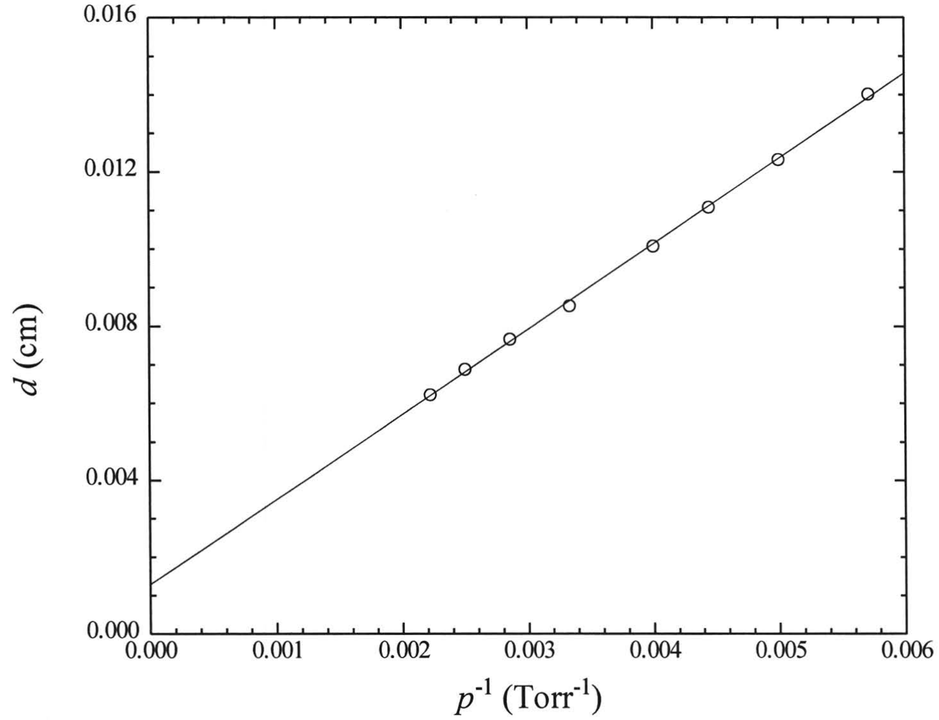

Figure 4.7: The size of the cathode fall d against the reciprocal pressure p^{-1}. A linear fit is made to represent the scaling law that the product $p{\cdot}d$ stays constant in changing p. This plot concerns the same simulation as Figure 4.6.

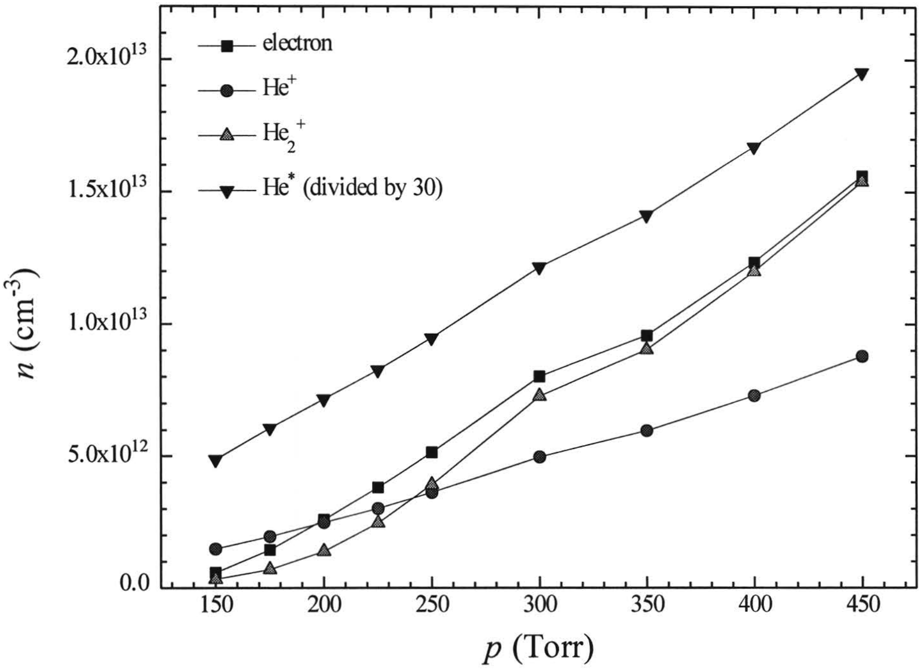

Figure 4.8: The maximum densities of the different species as a function of gas pressure. This figure concerns the same set of simulations as Figure 4.6.

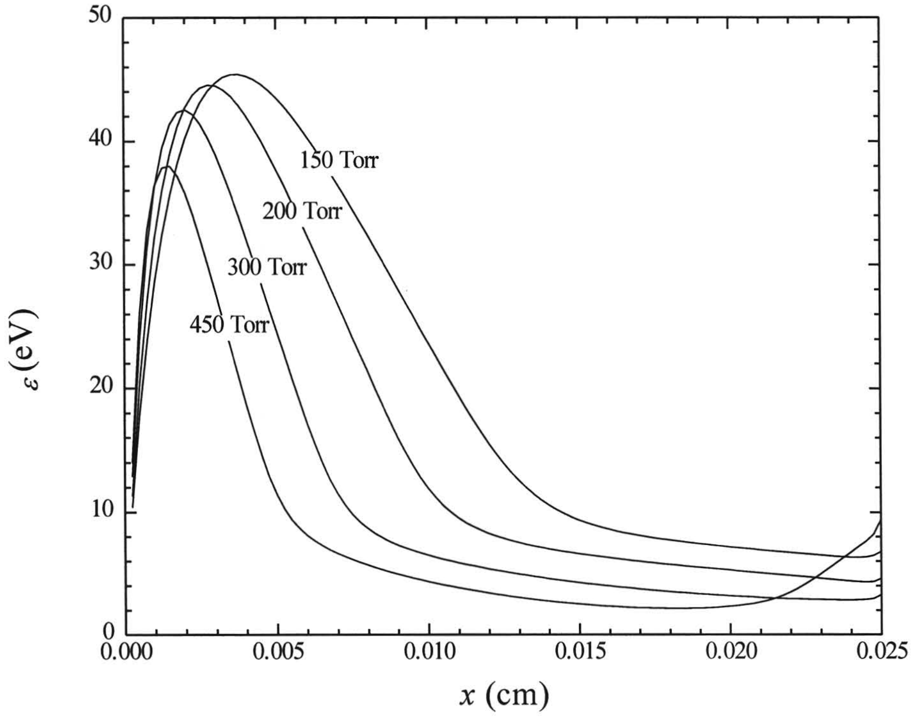

Figure 4.9: The electron mean energy profile for different pressures. This plot concerns the same simulation as Figure 4.6.

So far we applied our voltage directly to the discharge electrodes, without using an external electrical circuit. However, doing so can give problems in reaching a steady state. For instance, the calculations discussed above for both relatively high and low pressures do not reach a steady state if we use parabolic or sine-shaped initial density profiles. For high pressures (>300 Torr) the densities blow up to infinity and for low pressures (<200 Torr) all charged particles vanish completely. In these cases the calculations only converge into a real steady state if the initial density profiles are not too far from the steady state density profiles. (For example we can reach a steady state at 150 Torr if we use the steady state densities at 200 Torr as the initial densities for the calculation at 150 Torr.)

We can solve the problems in reaching a steady state by connecting a resistor in series with the discharge, as shown in Figure 4.10. If we choose an appropriate value for the series resistor, a useful feedback arises from the discharge current to the discharge electrode voltage. As the discharge current increases the electrode voltage decreases. We can now apply somewhat higher voltages without running the risk of blowing up the densities, which makes it much easier to reach a steady state.

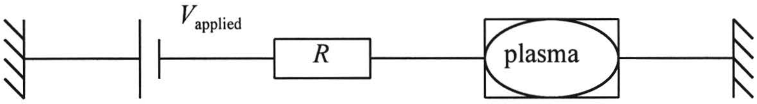

Figure 4.10: The discharged connected in series with a resistor.

The disadvantage of using a series resistor is, that it is no longer possible to control the electrode voltage directly. This makes it nearly impossible to study the influence of a particular parameter on the discharge characteristics. If you make a series of analogous simulations varying one particular parameter and apply every time the same voltage to the total circuit, you will get to do with a different voltage across the discharge for every value of the parameter you are varying. Hence you will not be examining the effect of this parameter alone, but a mixture of this effect and the effect of the discharge voltage. In other words, the series resistor becomes part of the discharge configuration, thus introducing an additional (and undesirable) degree of freedom. Nevertheless, we will use a series resistor in some of our DC discharge simulations, for it is hardly possible to study the influence of the secondary emission coefficient or to simulate helium-nitrogen mixtures without it. Moreover, in real experiments one also has to use a series resistor if one wants to create a stable DC discharge.

First we will demonstrate the influence of the electrode voltage by doing a series of simulations with different electrode voltages. In these simulations we use a gas pressure of 200 Torr and a value of 0.1 for the secondary emission coefficients of all heavy species. Figure 4.11 shows the densities of electrons and ions for different electrode voltages. It turns out that as the electrode voltage increases, the thickness of the cathode fall decreases and the plasma density increases. These facts result from an increasing probability of ionization and excitation due to an increasing electron mean energy. Figure 4.12 shows the discharge current density as a function of the discharge voltage.

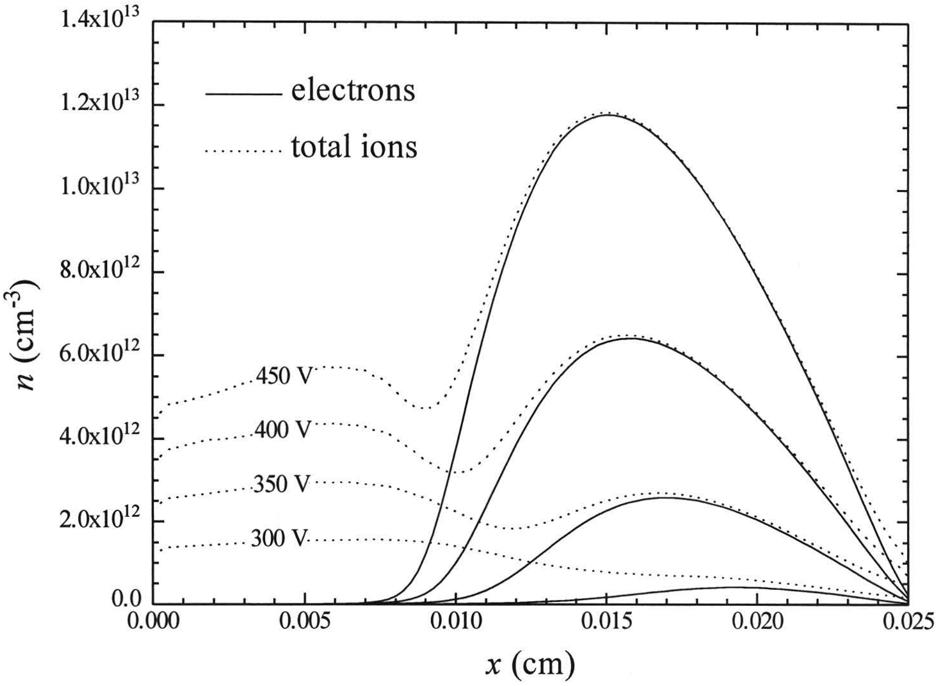

Figure 4.11: The density of electrons and the total density of ions as a function of position for different electrode voltages. The cathode is located on the left. The gas pressure is 200 Torr and the secondary emission coefficient is put to 0.1 for all heavy species.

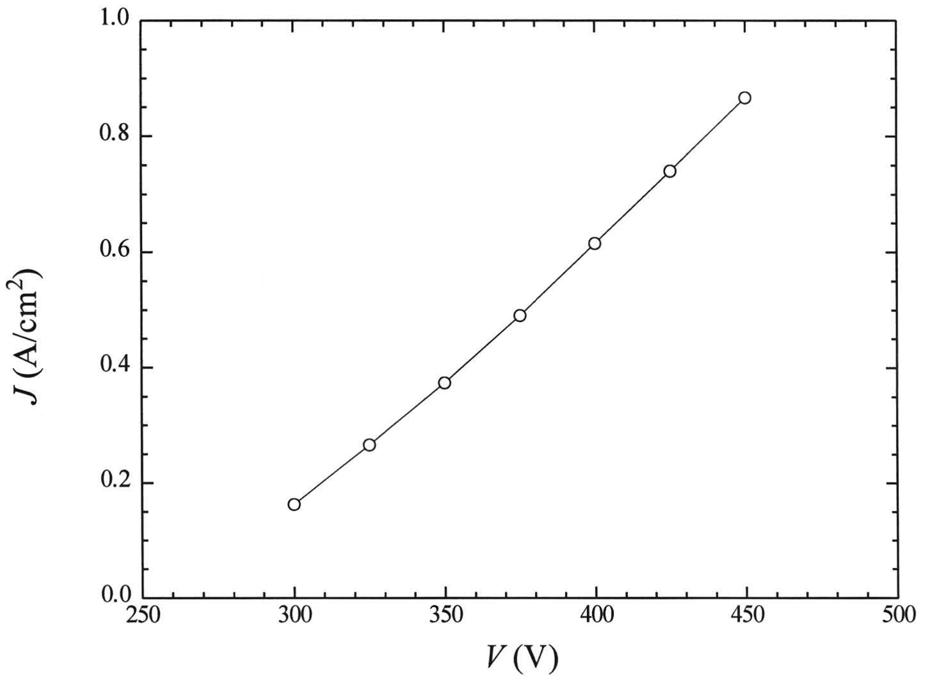

Figure 4.12: The current density as a function of the electrode voltage. This figure concerns the same series of simulation as Figure 4.11.

If we want to examine the influence of the secondary emission coefficient it is necessary to include a series resistor. We assume that the area of the electrodes is equal to 0.045 cm^2 and we use a resistor of 1650 Ω. (We use these values in analogy with an experimental setup, which is discussed in Section 4.7). We apply a voltage of 500 V across the total circuit. Figure 4.13 shows the density profiles of electrons and ions for different secondary emission coefficients. We take these secondary emission coefficients the same for all heavy species. The voltages across the discharge electrodes vary from 412.4 V (for $\gamma = 0.14$) to 490.6 V (for $\gamma = 0.02$).

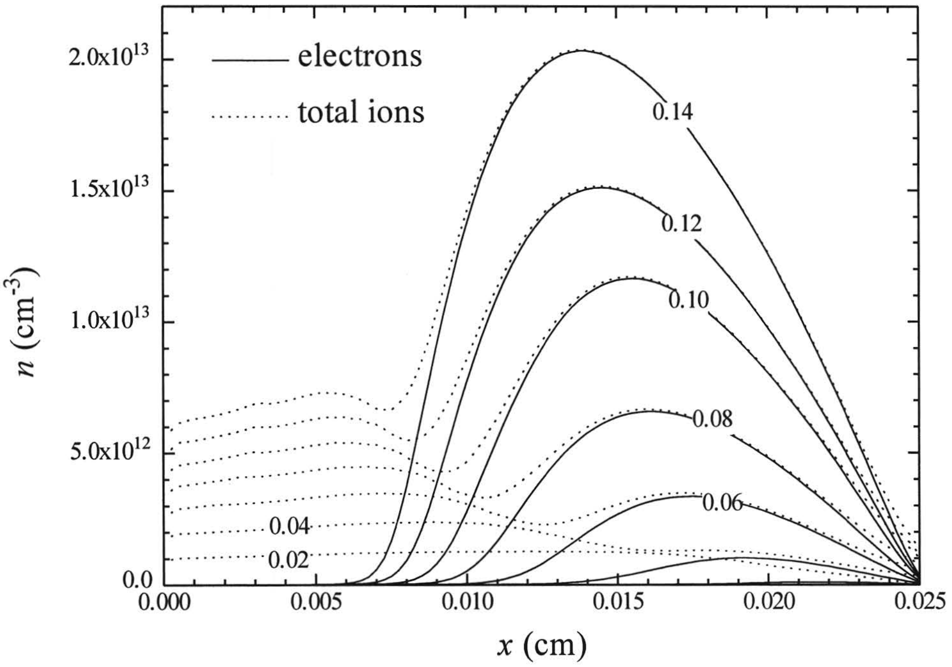

Figure 4.13: The density of electrons and the total density of ions as a function of position for different values for the secondary emission coefficient. The secondary emission coefficients are the same for all heavy species. The discharge is placed in series with a resistor of 74.25 Ωcm^2 , the applied voltage is 500 V and the cathode is located on the left. The gas pressure is 200 Torr.

4.3 DC DISCHARGES IN HELIUM-NITROGEN MIXTURES

Figure 4.14 displays the density profiles of all species in a DC discharge in a mixture of 99.8% helium and 0.2% nitrogen. Even though the percentage of nitrogen is quite small, by far the most abundant ions are the molecular nitrogen ions N_2^+. This results from the relatively high probability of the Penning reactions (3.17) and (3.18). Because the partial nitrogen pressure is low and the densities of the nitrogen species are relatively high (especially the density of N) it is sensible to verify if the percentage of nitrogen gas molecules that are turned into other species is negligible, in order to make sure that our assumption of constant gas pressure is justified. The maximum density of N is 2x10^{13}, which is indeed negligible compared to the density of nitrogen molecules at 0.2%·200 Torr 1.3x10^{16} cm^{-3}.

The influence of the nitrogen on the steady state densities is demonstrated more clearly by Figures 4.15 and 4.16, which show the density curves of charged particles and of helium metastables, respectively. There seems to be no straightforward relationship between the percentage of nitrogen and the plasma density or the size of the cathode fall. The helium metastable density decreases strongly with increasing percentage of nitrogen, reflecting again the importance of Penning ionizations.

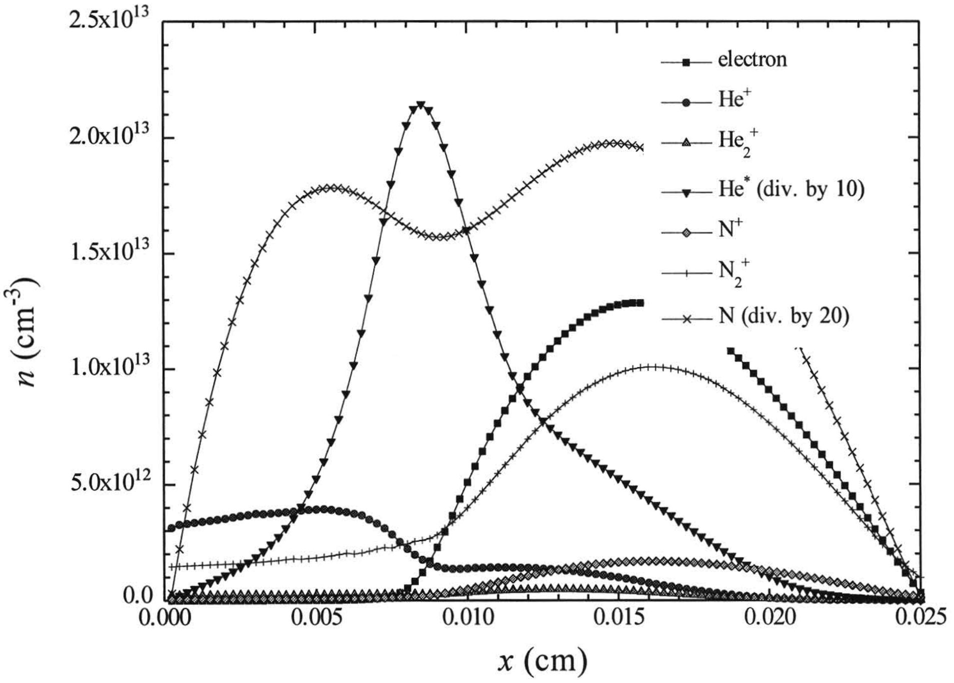

Figure 4.14: Density profiles of the different species in a DC discharge in a mixture of helium and 0.2% nitrogen. The gas pressure is 200 Torr, the secondary emission coefficient of all ions and metastables is 0.1. The discharge is in series with a resistor of 74.25 Ωcm^2 and the applied voltage is 500 V. The cathode is located at $x = 0$ and the anode at $x = 0.025$ cm. Notice that the densities of helium metastables and nitrogen atoms have been divided by 10 and 20, respectively.

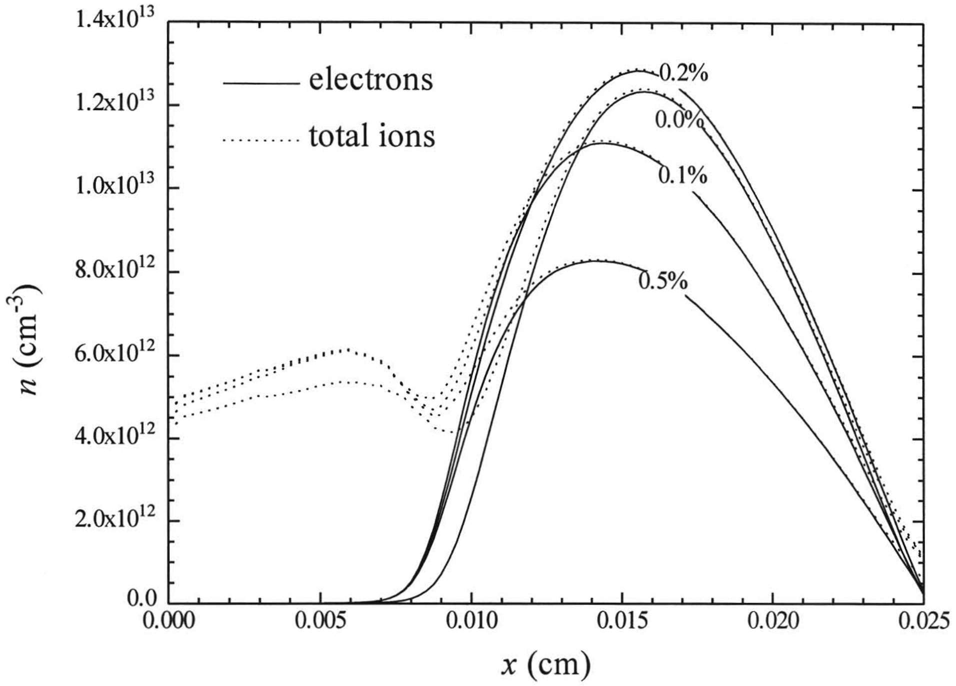

Figure 4.15: The density of electrons and the total density of ions as a function of position for different percentages of nitrogen. The discharge conditions are the same as in the simulation of Figure 4.14.

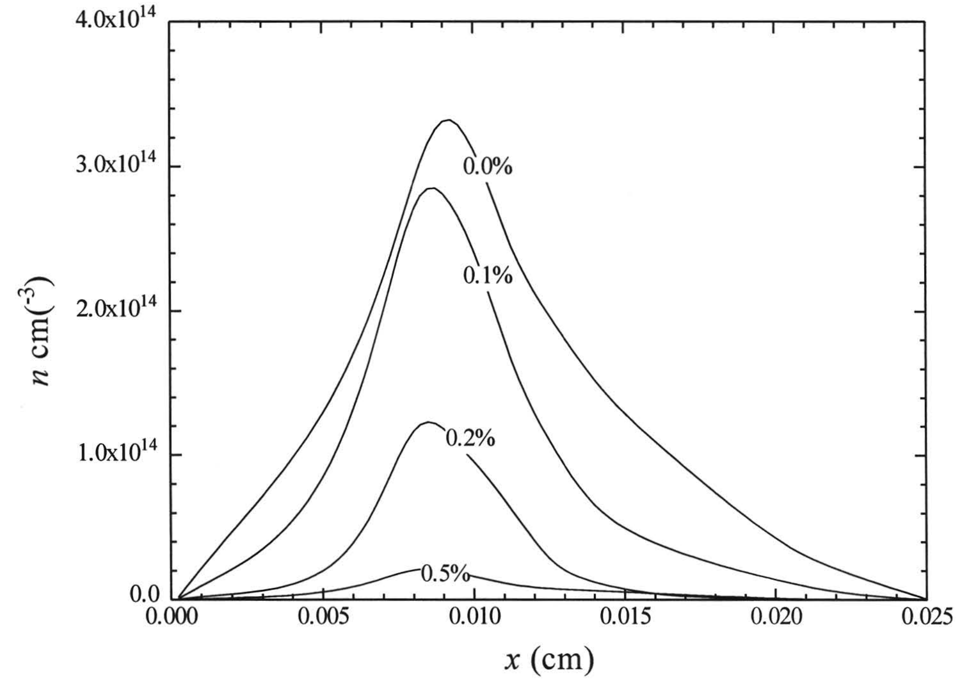

Figure 4.16: The density profile of helium metastables for different percentages of nitrogen. This plot concerns the same simulations as Figure 4.15.

4.4 AFTERGLOW

Up till now we studied only the steady state of DC discharges. We can also do afterglow simulations, which can give us an idea about the decay of the plasma in a PALC channel after a discharge pulse. For the afterglow simulations we consider an electrode distance of 0.01 cm, which is a typical value for the depth of a PALC channel. It makes sense to focus on the direction from the bottom to the top of the channel because the channel dimensions are the smallest in this direction, so that this direction is the dominant one for the diffusional decay (see equation (1.19)).

In a real PALC channel the top and the bottom wall are made of dielectric material, while in the model we have two walls of conducting material (electrodes). At first sight this seems to be a problem because the boundary conditions for dielectric material are different from those for electrodes. The potential of an electrode wall has a given value, whereas the potential of a dielectric wall is floating. The electric wall charge on an electrode is governed by the condition that the electric field is zero inside the electrode, whereas the wall charge on a dielectric wall is determined by the charged particles that have arrived at the wall in the past. However, this difficulty is merely appearance. Wall charges and wall potentials are not really important for our calculations. What really matters is the electric field, and this is determined by space charges and by the difference between the wall potentials. The absolute values of the potentials of the walls do not affect the electric field in the plasma at all. In our afterglow simulations we will put the potentials of both electrodes to zero, thus assuming a symmetric situation. In this case there is no difference between conducting or insulating walls. (If we want to simulate the charging of the liquid crystal layer at the top of a channel the wall charges will be important, but we will come to that later.)

For the initial densities we take sine-shaped profiles (diffusion profiles, see Section 1.5) with maximum values equal to the plasma densities of the steady state of the corresponding (preceding) discharge (Sections 4.1-4.3). Figure 4.17 shows the average densities as a function of time. In the first microsecond in the afterglow the densities of both He_2^+ ions and electrons increase, because of the metastable-metastable ionization process (3.8). The density of He^+ ions decreases rapidly due to the ion conversion reaction (3.7). It is obvious that there is ambipolar diffusion between He_2^+ ions and electrons. This ambipolar diffusion breaks when the densities become lower than about 10^{10} cm^{-3}. This value agrees with the criterion for ambipolar diffusion imposed by the Debye length. If we substitute $L = 0.01$ cm into equation (1.21) we obtain the demand that the densities must be greater than 8.5×10^9 cm^{-3} in order to maintain the ambipolar diffusion.

Figure 4.18 shows the decreasing electron temperature in the afterglow. After 0.2 microseconds the electrons have cooled down to the gas temperature of 300 K. Notice that it is very important to observe the correct values for the electron diffusion coefficient at low electron temperature in the calculation. This diffusion coefficient is calculated from the mobility by application of the Einstein relation (2.61). One could easily overlook the fact that the mobility of thermalized electrons is about one order of magnitude larger than the electron mobility at higher electron energy (Figure 3.3) and obtain totally inaccurate results.

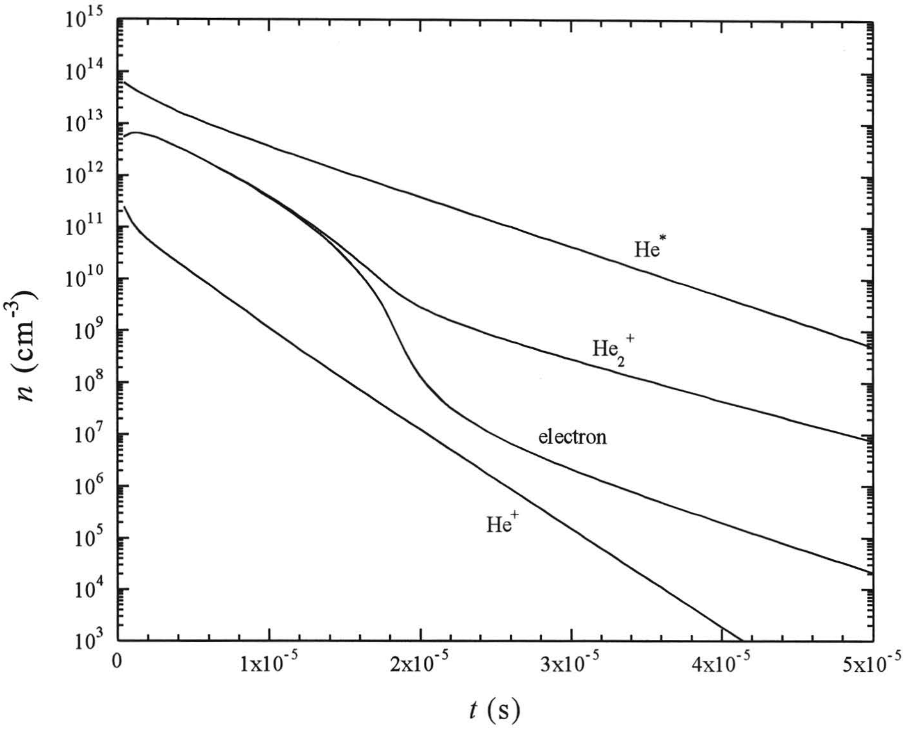

Figure 4.17: Space averaged densities of the different species as a function of time in a pure helium afterglow. The gas pressure is 200 Torr.

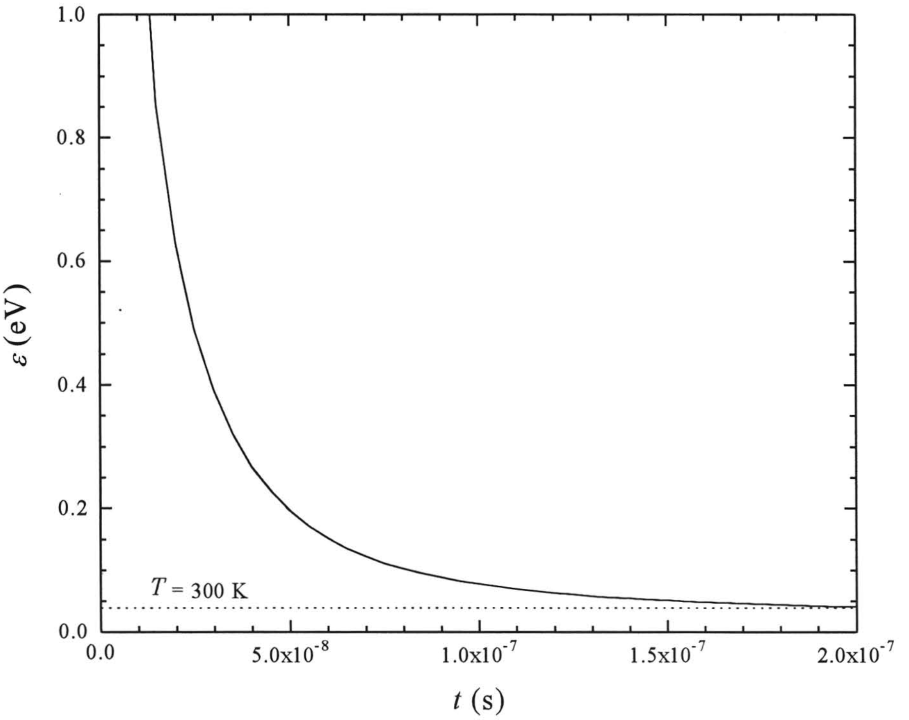

Figure 4.18: Position averaged electron mean energy as a function of time in a pure helium afterglow. This plot concerns the same simulation as Figure 4.17.

Figures 4.19 and 4.20 displays the charged particle densities and the metastable density, respectively, as a function of time for different gas pressures. The decay of the plasma is slower as the pressure is higher.

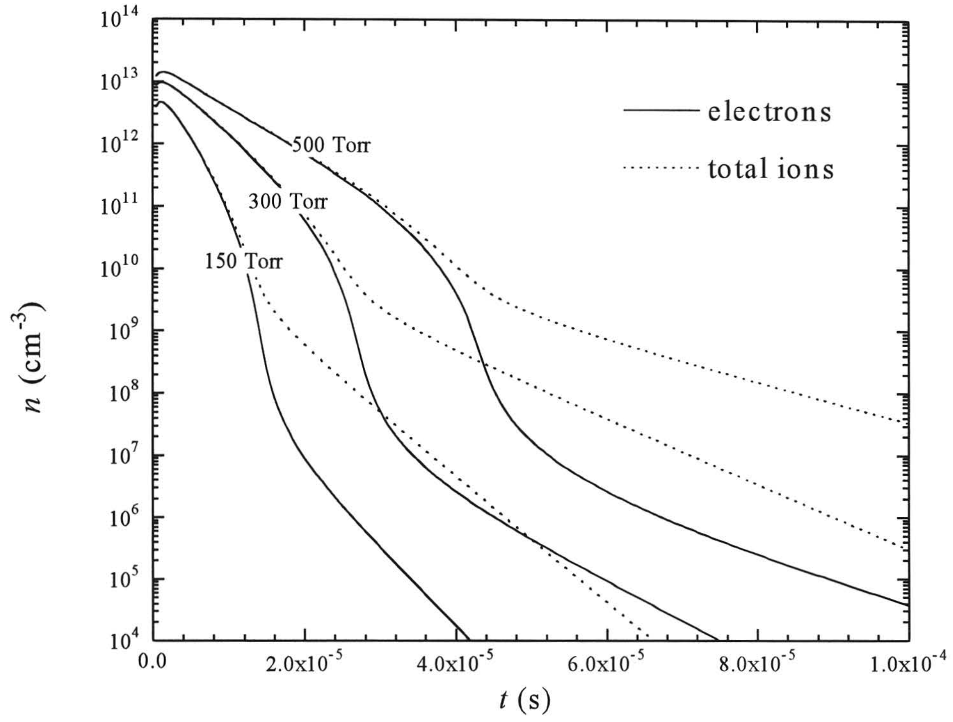

Figure 4.19: Space averaged densities of electrons and ions as a function of time in a pure helium afterglow for different gas pressures.

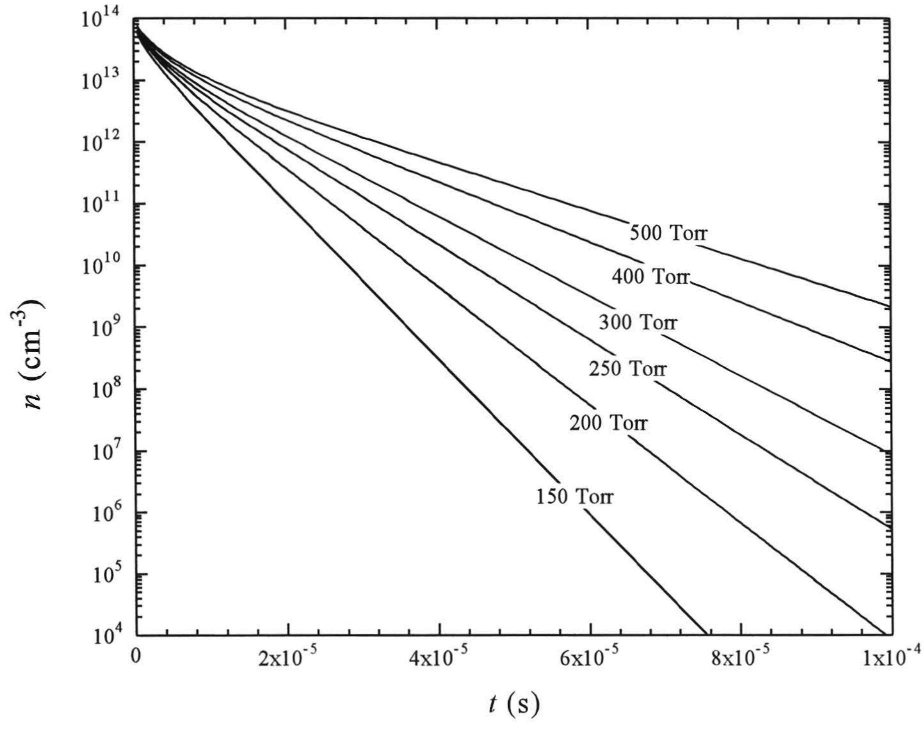

Figure 4.20: Space averaged metastable density as a function of time in a pure helium afterglow for different gas pressures.

The densities in the afterglow in a mixture of helium and 0.2% nitrogen are depicted in Figure 4.21. Both helium ion species disappear quickly due to the ion conversion reactions (3.13)-(3.16). The most important ion is N_2^+. The decay of the charged particle densities is much faster than in a pure helium discharge. This effect is illustrated in Figure 4.22, which shows the decay curves of the electron and ion densities for different percentages of nitrogen. The main reason for the faster decay in helium-nitrogen mixtures is the fact that the helium metastables, which prolong the pure helium afterglow by their (relatively slow) metastable-metastable ionizations, are removed quickly by Penning ionizations (3.17) and (3.18). Figure 4.23 displays the decay curves of these helium metastables for different percentages of nitrogen.

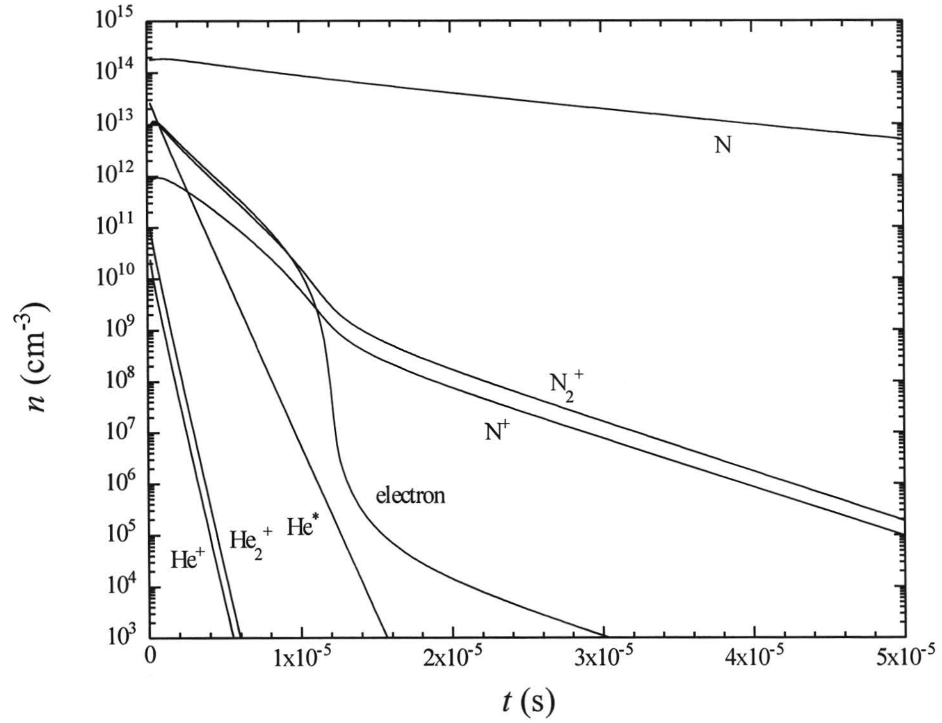

Figure 4.21: Space averaged densities of the different species as a function of time the afterglow in mixture of helium and 0.2% nitrogen. The gas pressure is 200 Torr.

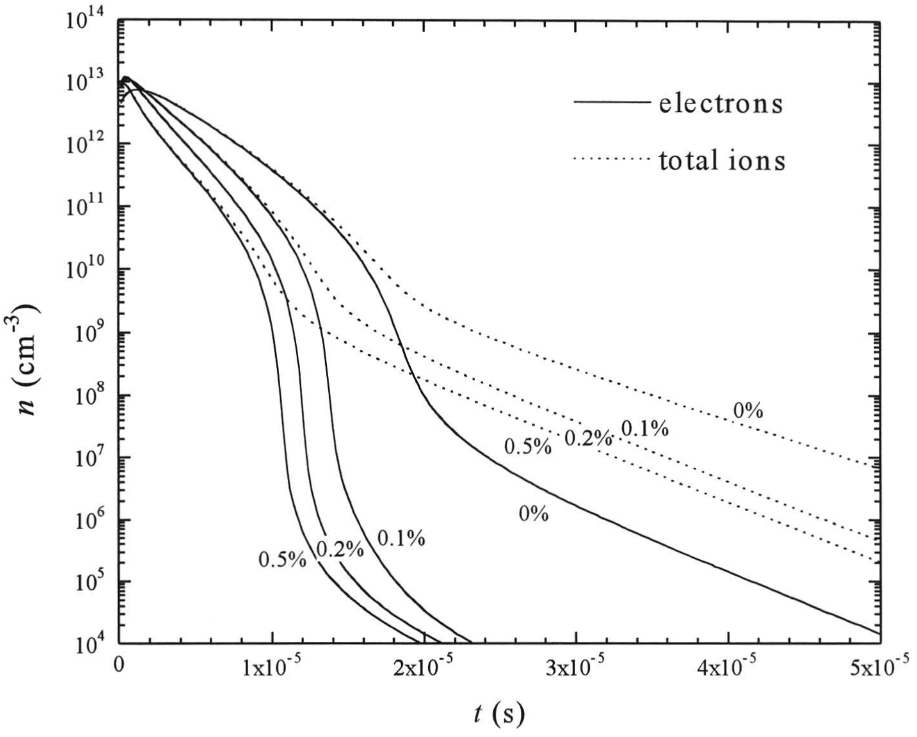

Figure 4.22: Space averaged densities of electrons and ions as a function of time in the afterglow in a helium-nitrogen mixture for different percentages of nitrogen. The gas pressure is 200 Torr.

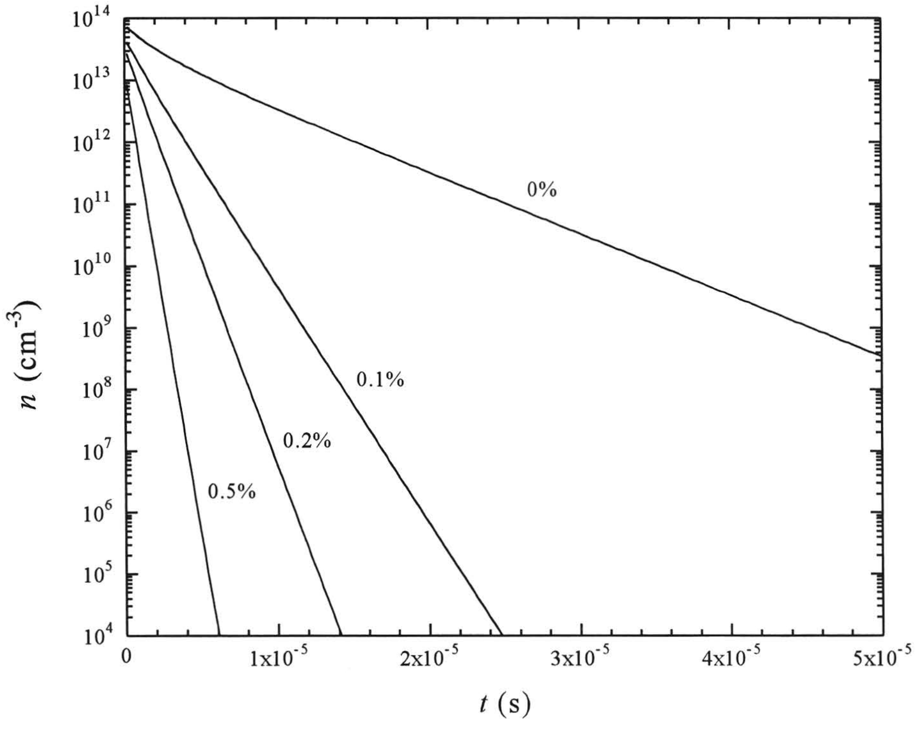

Figure 4.23: Space averaged densities of helium metastables as a function of time in the afterglow in a helium-nitrogen mixture for different percentages of nitrogen. The gas pressure is 200 Torr.

4.5 ADDRESSING AND AFTERGLOW

In this section we attempt to simulate the charging of the liquid crystal layer as a result of the addressing of the data-electrodes (see Section 1.2). We will focus again on the direction from the bottom to the top of the channel. The liquid crystal layer (plus the protecting micro-sheet) can now be modeled as a capacitor, in series with the plasma.

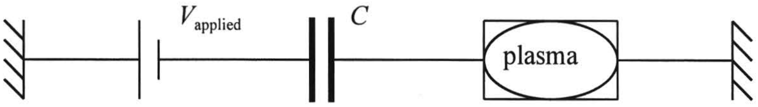

Figure 4.24: A capacitor can be connected in series with the plasma in order to represent the liquid crystal layer.

A typical capacitance for a liquid crystal layer is 150 pF/cm^2. We apply a certain small voltage (the addressing voltage) to the circuit during the afterglow. In the very beginning the addressing voltage produces a current through the plasma. The charges of this current accumulate on the capacitor. The charging of the capacitor continues until the entire addressing voltage is across the capacitor. After that the plasma decays like in the afterglow simulations we discussed before.

It turns out that the charging phase lasts only very short and has almost no influence on the decay of the plasma, as is to be expected from the following straightforward calculation. If the addressing voltage is 10 V, which is a typical value, the electric charge needed to fully charge the capacitor of 150 pF/cm^2 amounts to $Q = 10 \cdot 1.5\text{x}10^{-10} = 1.5\text{x}10^{-9}$ C/cm^2. This corresponds to $1.5\text{x}10^{-9}/1.6\text{x}10^{-19} \approx 10^{10}$ charged particles per cm^2. Typical electron and ion densities in the beginning of the afterglow are 10^{13} cm^{-3} (see Figures 4.17, 4.19). The number of charged particles between the electrodes (electrode distance 0.01 cm) is then 10^{11} per cm^2, which is one order of magnitude larger than the number of particles on a charged capacitor.

In the PALC technology one wants the liquid crystal layer to remain charged after switching off the addressing voltage. It is therefore interesting to see what happens to our capacitor if we switch off the addressing voltage after a certain time (we will call this the addressing time). At the moment we do this, a voltage opposite to the addressing voltage comes across the plasma electrodes. The charged particles that are still present in the gas start to drift and neutralize the charges on the capacitor. Figure 4.25 shows the particle densities and the voltage across the capacitor as a function of time for the case that the addressing voltage of -10 V is switched off after 10 μs in the afterglow. The electrons and ions are almost entirely pulled away by the electric field. They are not able to neutralize the charges on the capacitor completely in this case; a voltage of -4 V remains present across the capacitor.

The extent to which the capacitor is discharged after turning off the addressing voltage depends on the addressing time. Figure 4.26 displays the percentage of the original addressing voltage that is eventually left across the capacitor, as a function of the addressing time and for different addressing voltages. For short addressing times (<7 μs), there are still many charged particles and metastables present in the gas so that the capacitor is discharged completely after switching off the addressing voltage.

In order to keep the greater part of the addressing voltages across the capacitor we need to wait until the plasma is almost totally gone before turning it off (> 20 μs). Lower addressing voltages require a longer addressing time, as can be seen in Figure 4.26.

There also appears to be an influence of the polarity of the addressing voltage, especially for low addressing voltages. This can be explained as follows. If we apply a negative addressing voltages, the positive charges of the plasma (the ions) will be pulled upon the capacitor. After switching off the voltage it will be the plasma electrons that discharge the capacitor again. On the other hand if we use a positive addressing voltage it will be the plasma ions that are responsible for the discharging of the capacitor. The difference is now, that after the ambipolar diffusion is broken the electrons decay faster than the ions (see Figure 4.17). Notice that not only the electrons and the ions, but also the metastables are of importance. Most metastables are eventually turned into charged particles.

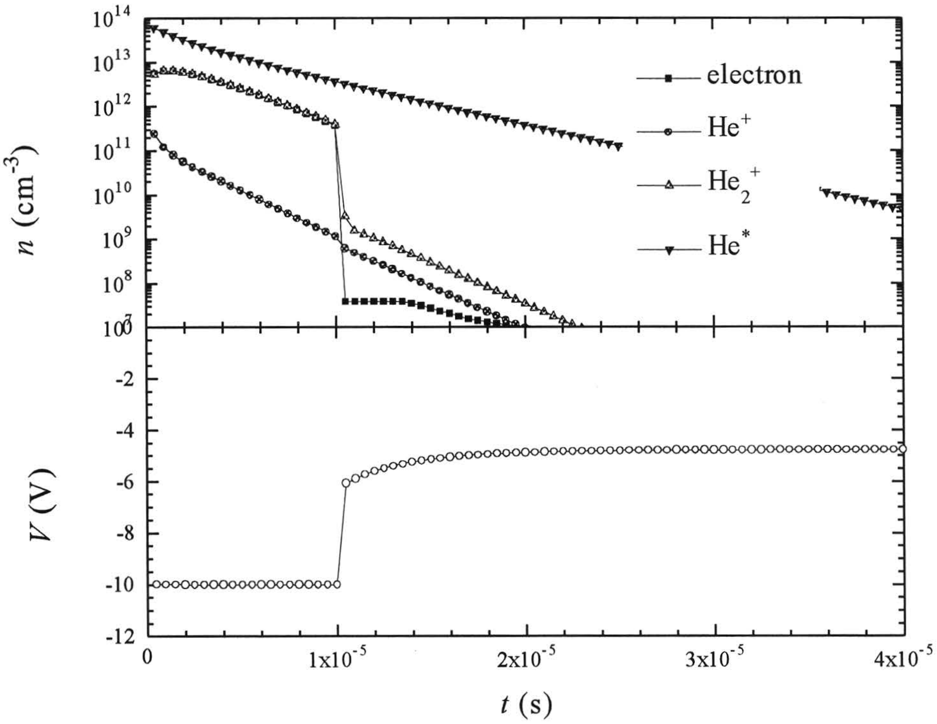

Figure 4.25: The particle densities and the voltage across a series capacitor of 150 pF/cm^2 as a function of time in the afterglow. An addressing voltage of -10 V is applied to the total circuit during the first ten microseconds.

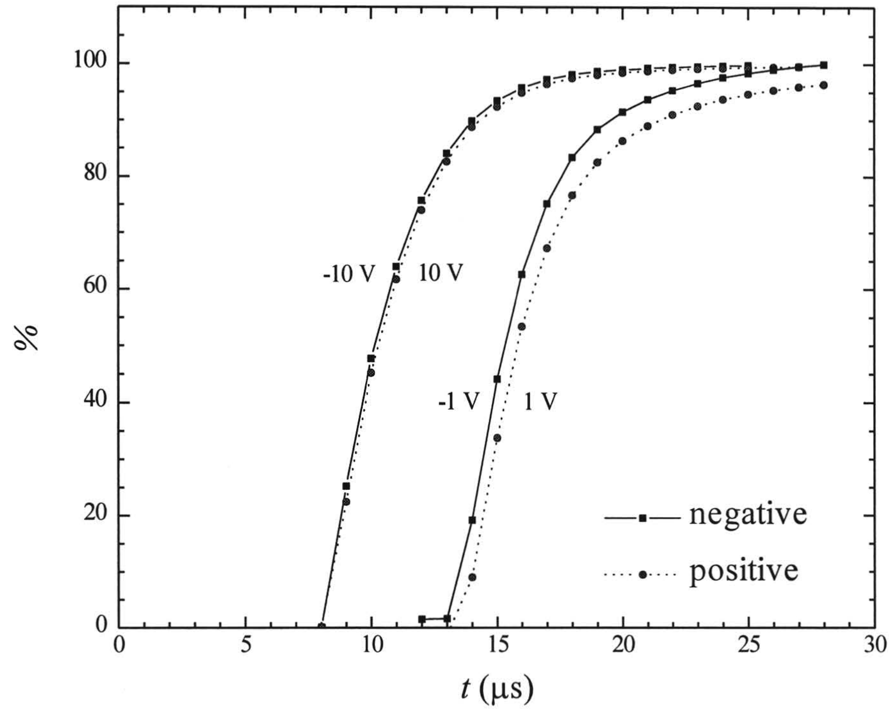

Figure 4.26: The percentage of the addressing voltage that is eventually left across the capacitor after switching off the applied addressing voltage, as a function of addressing time for different addressing voltages.

4.6 COMPARISON TO EXPERIMENTAL RESULTS

In this section we will compare some simulation results to experimental measurements on a test-panel. The dimensions of the channels of this test-panel are the dimensions indicated in Figure 4.1. The length of the channels is 9 cm. In the test-panel there are no data-electrodes or liquid crystal layer present.

The micro-discharges in the test-panel can be studied with optical diagnostics. Using a microscope it is possible to measure the intensity the 587.56 nm line as a function of the position between the electrodes. Light of this wavelength is emitted by the discharge as a result of the decay of the He(3 D) excited state to a lower energy level. The result of such a measurement is depicted in Figure 4.27.

Let us assume that the He(3 D) state is populated mainly by the electronic excitation of ground state helium atoms and decays instantaneously

$$\mathrm{He} + e^- \rightarrow \mathrm{He(3\ D)} + e^-$$
$$\mathrm{He(3\ D)} \rightarrow \mathrm{He(2\ P)} + 587.56\ \mathrm{nm}$$

In this case the light emission profile is an image of the electron excitation rate for the He(3 D) level. We implement this excitation reaction into the model code (without further considering the resulting excited species). The excitation coefficient is calculated by BOLSIG and looks much like the coefficients for the excitation of the helium metastables (Figure 3.5). Figure 4.27 also displays the simulation results for the electronic excitation rate of He(3 D). The curves obtained by measurement and by simulation are not completely comparable because they concern different discharge

voltages. In the experiment the voltage across the electrodes is 267 V but unfortunately a calculation with this voltage suffers from instabilities in the electron temperature so that we have to use a somewhat higher voltage.
The general shape of both curves is the same. Going from cathode to anode the excitation rate first increases, mainly due to the increasing electron density, and then decreases again due to decreasing electron energy. It is conspicuous that the emission in the plasma is much bigger than one would expect from the simulation. This fact raises doubts about the validity of our assumption that electronic excitation of ground state helium atoms is the only process which populates the He(3 D) level. Further excitation of metastable atoms might also be important. (Unfortunately we could not find cross-section or reaction coefficients for this process.) Another possible explanation is that the electron temperature in the plasma is higher in reality than in the (one dimensional) simulations.

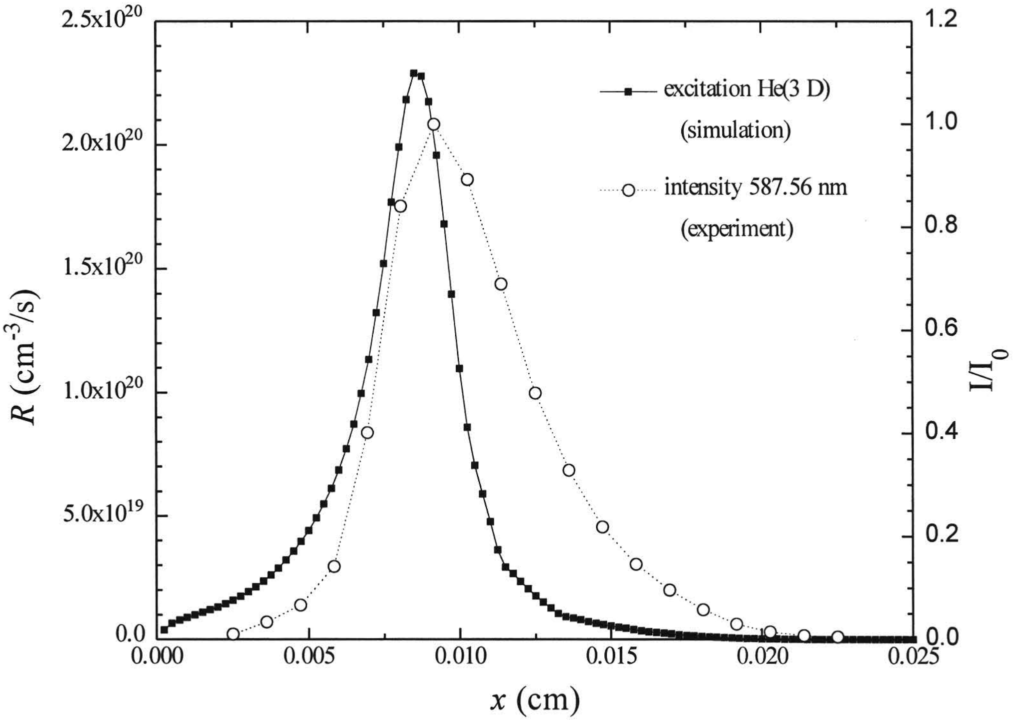

Figure 4.27: The reaction rate of electronic excitation of He to the He(3 D) level as obtained by a simulation (scale right) and the relative intensity of the 587.56 nm line (which may result from the decay of He(3 D)) as measured in an experiment (scale left), both as a function of position. The cathode is located on the left. Both curves are not entirely comparable for the simulated curve is obtain with a electrode voltage of 300 V, while in the experiment the sustaining voltage is 267 V.

We can also compare our simulations to electrical measurements on the test-panel. The big problem for this comparison is that in our one dimensional calculations we work with a current density. This quantity can only be compared with an experimentally measured current if we know the electrode surface area covered by the discharge. However, it turns out to be impossible to find a good and unambiguous value for this area. The currents that one calculates using the total electrode area of 0.045 cm^2 are smaller than the measured currents, even if one uses very high values for the secondary emission coefficients. This suggests that the real discharge is broader than the electrodes (see Figure 4.28). To calculate currents in a proper way one needs a two dimensional model.

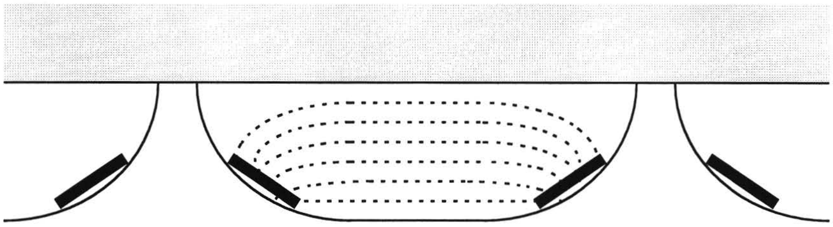

Figure 4.28: The discharge in the channel might be broader than the electrodes.

The afterglow can be studied experimentally by electrical measurements. During the afterglow a small voltage (20 V) is applied to the channel electrodes. The resulting current is measured. This current turns out to be decaying in an exponential way. The time constant of this decay is called the "afterglow time". Although we cannot obtain proper currents from our simulations, we can compare calculated afterglow times to measurements. We simulate the experiments using an electrode distance of 0.025 cm and an applied voltage of 20 V. We take steady state discharge density profiles (Sections 4.1-4.3) for initial densities. In the beginning of the afterglow the current density turns out to decay exponentially indeed. Table 4.1 compares the simulated decay times to the measured afterglow time for different percentages of nitrogen. The simulated times are about twice as long as the measure times. This is to be expected since in the one dimensional calculations we do not take into account diffusion towards the top and the bottom of the channel. In reality these losses are probably even more important than the losses towards the electrodes.

Table 4.1: Calculated and measured afterglow times in helium nitrogen mixtures. The applied voltage during the afterglow is 20 V. In the calculations we used the density steady state profiles discussed in Section 4.3 as initial conditions.

% N_2	τ (μs) calculated	τ (μs) measured
0	4.16	1.84
0.1	2.31	1.30
0.2	1.53	0.98
0.5	1.13	0.58

4.7 SCALING

In Section 4.2 we saw that the scaling law that $p{\cdot}d$ is constant in similar discharges is supported by the modeling results for gas pressures in the range of 175-450 Torr. It is interesting to see if the scaling law is also valid for scaling over orders of magnitude. In order to study this, we will simulate a discharge with exactly the same conditions as the discharge discussed in Section 4.1, but then a hundred times larger (2.5 cm instead of 0.025 cm) and with a pressure of a hundred times smaller (2 Torr instead of 200 Torr). So we scale up the discharge of Section 4.1 with a factor $a = 100$ to obtain

a discharge of "normal" dimensions. We remark that our kinetic model (Section 3.2) is designed for high pressures and could be inaccurate for low pressures.
Figure 4.29 shows the density profiles of the different species. This figure can be compared to Figure 4.2. It turns out that the discharge is indeed similar. The relative size of the cathode fall is the exactly same. The densities of the charged species are 10^{-4} ($= a^{-2}$) times the densities in the similar micro-discharge, in agreement with equation (1.4). On the other hand the density of the metastables is only 1000 times smaller. This is to be expected from the following consideration. The metastables are created by excitation and lost mainly by metastable-metastable ionization (3.8). So the rates of these two reactions must be approximately equal to each other. The excitation rate $R \propto [e^-][He] \propto a^{-3}$ and the metastable-metastable ionization rate $R \propto [He^*]^2$. Equating these to rates gives $[He^*] \propto a^{-3/2} = 10^{-3}$.
Notice that even at a pressure of 2 Torr the He_2^+ ion play an important part. This seems to be contradictory to our observation in Section 4.2 that the relative abundance of He_2^+ is positively correlated with the gas pressure (see Figure 4.8). However, this positive correlation is only true for high pressures, because only in high pressures the most important creation process for He_2^+ is the three-body ion conversion reaction (3.7). At lower densities most He_2^+ ions are created in metastable-metastable ionizations.
Figure 4.30 displays the electron mean energy. This energy is exactly the same as the energy in the similar micro-discharge (Figure 4.3). The current density through the discharge is $J = 3.90\text{x}10^{-5}$ cm^{-2}/s, which is about 10^{-4} ($=a^{-2}$) times the current density in the micro-discharge of Section 4.1 ($J = 0.374$ cm^{-2}/s, see Figure 4.12), in accordance with equation (1.12).

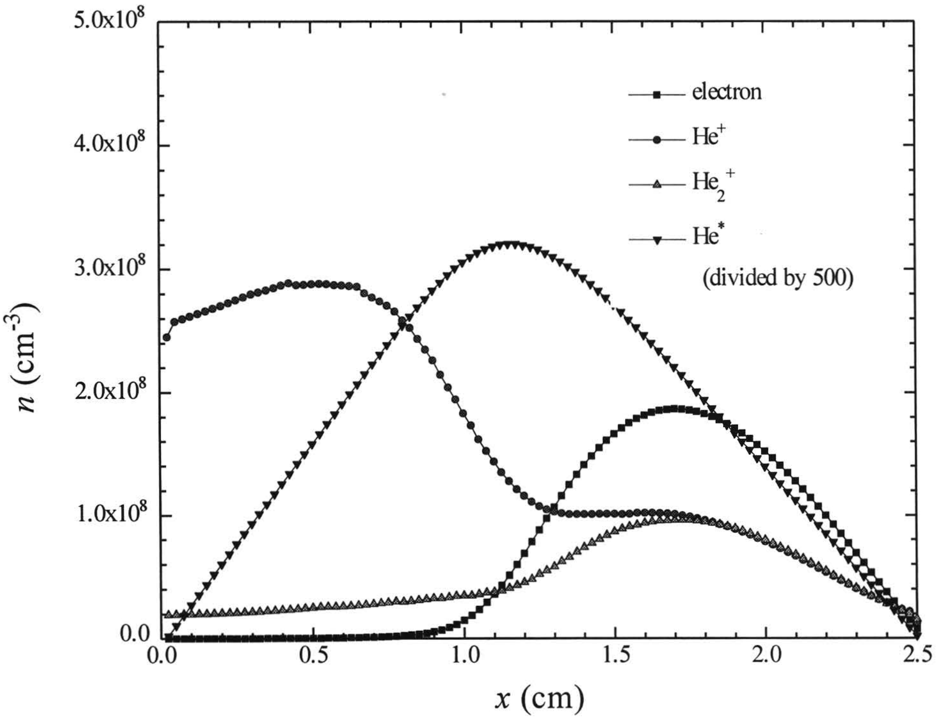

Figure 4.29: Density profiles in a "normal dimension" DC discharge in pure helium. The gas pressure is 2 Torr. Notice that the density of metastables is divided by 500. This figure can be compared directly with Figure 4.2.

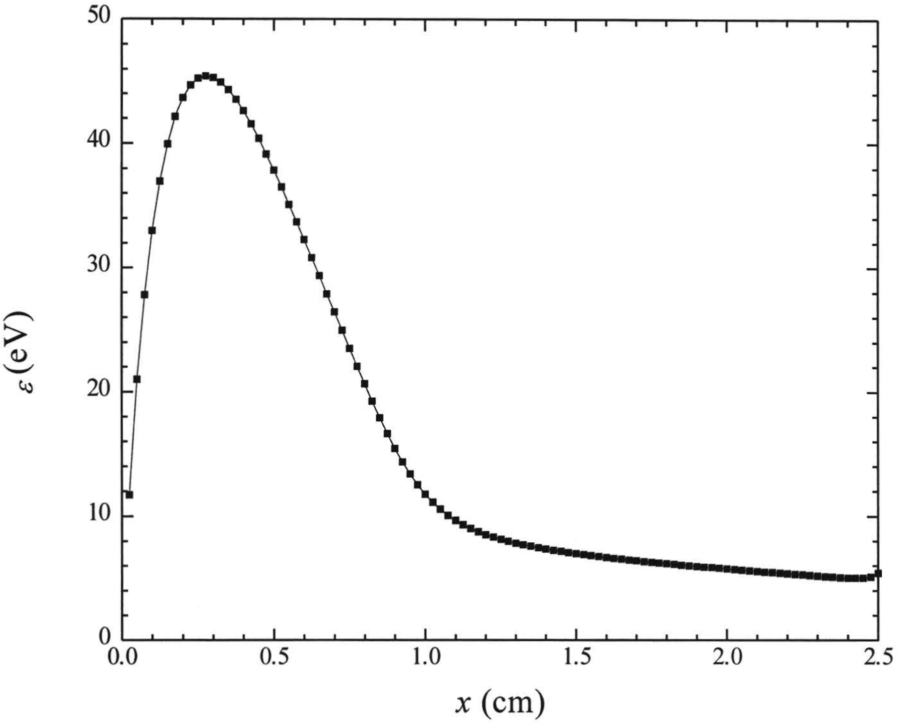

Figure 4.30: The electron mean energy in a "normal dimension" DC discharge. This figure concerns the same simulation as Figure 4.30 and can be compared directly to Figure 4.3.

Finally we simulate an afterglow at "normal" dimensions. We scale up the first afterglow simulation discussed in Section 4.4 by a factor $a = 100$. The distance between the electrodes is now 1 cm and the gas pressure is again 2 Torr. For the initial densities we take sine-shaped profiles with maximum values equal to the plasma densities of Figure 4.29. The decay curves are presented in Figure 4.31. This figure can be compared to Figure 4.17. It turns out that the decay times are about 100 (=a) times the decay times in the micro-afterglow of Figure 4.17. This result is to be expected if we consider equation (1.19). The diffusion decay time is proportional to the square of the electrode distance and inversely proportional to the diffusion coefficient, $\tau \propto L^2/D \propto L^2 \cdot p \propto a$. The atomic ion He^+ is about equally abundant as the molecular ion He_2^+, which is in contrast with the fact that the He_2^+ ion is by far the most important ion in the micro-afterglow. The explanation for this is that the three-body ion conversion reaction (3.7), which is responsible for the rapid vanishing of He^+ in the micro-afterglow, is very unlikely at low pressures.

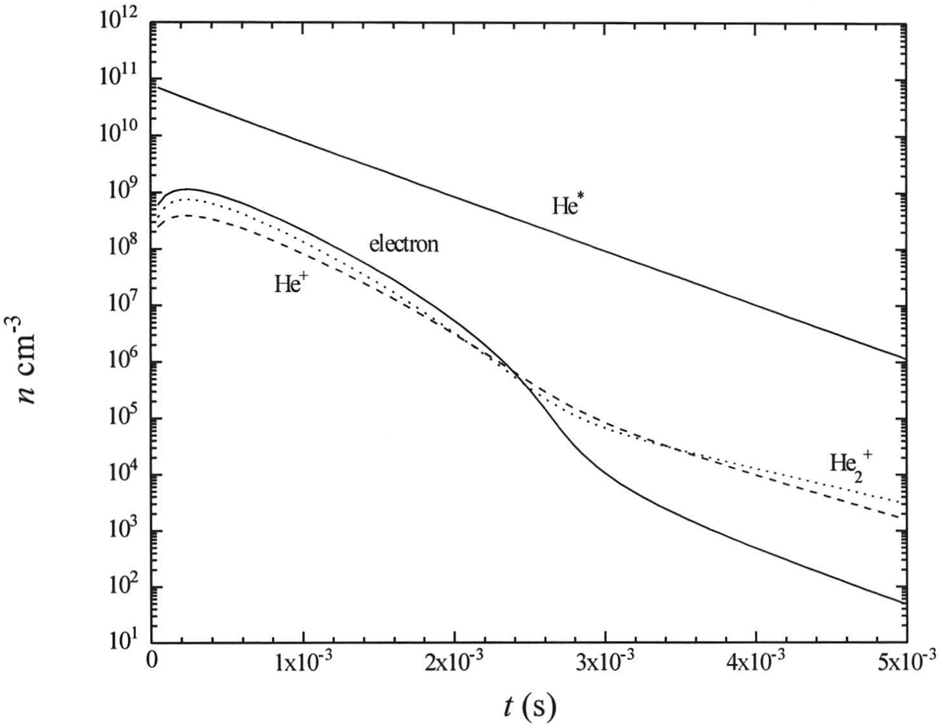

Figure 4.31: Space averaged densities of the different species as a function of time in a "large" afterglow. The gas pressure 2 Torr. This figure can be compared with Figure 4.17.

4.7 Scaling

5 GENERAL CONCLUSIONS

In this chapter we will line up the most important conclusions drawn in the preceding chapter.

- The results of simulations of one dimensional DC micro-discharges display clearly a cathode fall region and a plasma (glow) region. The size of cathode fall is typically about one third of the electrode distance. The plasma density is positively, the thickness of the cathode fall negatively correlated with the gas pressure, the electrode voltage, and the secondary emission coefficients. The most abundant ion in the cathode fall in both pure helium and helium-nitrogen mixtures is He^+. In the plasma of a pure helium micro-discharge the He_2^+ ion is at least as abundant as the He^+ ion; its importance increases with increasing pressure. In the plasma of a helium-nitrogen mixture the dominant ion is N_2^+, even at nitrogen percentages as low as 0.1. The density of helium metastables decreases strongly with increasing percentage of nitrogen.

- According to the simulations the electron temperature in the cathode fall of a DC helium discharge amounts to 30 eV, in the plasma it is about 4 eV. The calculated electron energy profile demonstrates that it is necessary to take into account the energy equation for electrons in the model. The assumption we use in the model that the electron velocity is isotropic might be dangerous in the cathode fall.

- The results of simulations of one dimensional micro-afterglows display clearly the breaking of the ambipolar diffusion. In the afterglow in pure helium by far the most important ion is He_2^+, in helium-nitrogen mixtures the nitrogen ions N_2^+ and N^+ are dominant. The decay of the plasma in pure helium is governed by helium metastables, which produce charged particles by their helium metastable-metastable ionizations, thus dragging out the afterglow. In helium-nitrogen mixtures the helium metastables are removed quickly by Penning ionizations, and the plasma decay time decreases strongly with increasing percentage of nitrogen. This observation is supported by experimental data.

- The simulation results agree with classical theories about glow discharges and afterglows. The electric field in the cathode fall is approximately linear and the the product $p{\cdot}d$ is constant. Classical scaling laws seem to apply reasonably well for scaling from micro-dimensions (0.01 cm) to normal dimensions (1 cm).

- It is possible to simulate the charging of the liquid crystal layer as a result of the addressing of the data electrodes. The charging itself turns out to occur very fast and easily, and has almost no influence on the decay of the plasma. The addressing time needed to keep a certain percentage of the charges on the liquid crystal may depend on the polarity of the addressing voltage; positive addressing voltages require longer addressing times than negative ones.

- To take into account diffusion to the bottom and the top of the channel during a discharge in a proper way, two dimensional modeling is required. This diffusion is probably not very important, but also not quite negligible. Two dimensional modeling is also required for the calculation of discharge currents, which can be compared with electrical measurements. Moreover, two dimensional modeling is desirable in order to make more realistic simulations of the charging of the liquid crystal layer and to be able to study the homogeneity of this charging.

APPENDIX

A GAUSS ELIMINATION

We have a system of linear equations of the following form

$$\begin{cases} b_0 x_0 + c_0 x_1 = d_0 \\ a_i x_{i-1} + b_i x_i + c_i x_{i+1} = d_i \qquad n > i > 0 \\ a_n x_{n-1} + b_n x_n = d_n \end{cases} \tag{A.1}$$

a_i, b_i, c_i and d_i are constant coefficients and x_i are unknowns. The x_i can be most easily solved by the Gauss elimination method. This method will be described here. We can rewrite the first equation

$$x_0 = \frac{d_0}{b_0} - \frac{c_0}{b_0} x_1 \tag{A.2}$$

and substitute this into the second one

$$\left(b_1 - \frac{c_0}{b_0} a_1\right) x_1 + c_1 x_2 = \left(d_1 - \frac{d_0}{b_0} a_1\right) \tag{A.3}$$

We now make the transformation

$$\begin{aligned} b_1 &\to b_1 - \frac{c_0}{b_0} a_1 \\ d_1 &\to d_1 - \frac{d_0}{b_0} a_1 \end{aligned} \tag{A.4}$$

Equation (A.3) becomes

$$b_1 x_1 + c_1 x_2 = d_1 \tag{A.5}$$

which can be rewritten as

$$x_1 = \frac{d_1}{b_1} - \frac{c_1}{b_1} x_2 \tag{A.6}$$

This again can be substituted in the third equation. We proceed like this through the equations from $i = 1$ to $i = n$, every time making the transformation

$$\begin{aligned} a_i &\to 0 \\ b_i &\to b_i - \frac{c_{i-1}}{b_{i-1}} a_i \\ c_i &\to c_i \\ d_i &\to d_i - \frac{d_{i-1}}{b_{i-1}} a_i \end{aligned} \tag{A.7}$$

Finally, we obtain for the last equation

$$b_n x_n = d_n \tag{A.8}$$

So we can calculate x_n and substitute it in the last equation but one

$$x_{n-1} = \frac{d_{n-1} - c_{n-1} x_n}{b_{n-1}} \tag{A.9}$$

We can work down through our equations like this from $i = n$-1 to $i = 0$, and calculate every x_i

$$x_i = \frac{d_i - c_i x_{i+1}}{b_i} \tag{A.10}$$

B CROSS-SECTIONS

The physical quantity that describes the probability of collisions is the cross-section. The dimension of cross-section is that of area. The cross-section is a measure for the chance that one specific particle “hits” another particle. In general cross-sections depend on the velocity of the particles in question. We can distinguish different cross-sections for different kinds of collisions. For instance, (chemical) reactions between particles can be regarded as collisions and be characterized by cross-sections. The cross-section of some particular reaction can depend strongly on the velocities of the reactants. However, in fluid theory we usually do not distinguish between particles with different velocities; we just characterize a particle species by a mean particle energy. (The mean energy is directly related to the mean absolute velocity.) In this approximation we do not work with cross-sections (which depend on the velocities of individual particles) but with reaction rate coefficients. The reaction (rate) coefficient is defined as the number of reactions per unit time per unit of density of the reacting particles. It can be calculated from the cross-section by integration over the velocity distributions of the reactants. In the case of a reaction between an electron and a heavy particle (ion or atom) we usually neglect the velocity of the heavy particle. In this case the reaction coefficient is given by

$$k = \langle \sigma v \rangle = \int_0^\infty \sigma(v) f(v) v dv \tag{B.1}$$

where k is the reaction coefficient, σ the cross-section which is a function the absolute electron velocity v only. $f(v)$ is the velocity distribution function (which is related to the mean particle energy). It is defined such that $f(v)dv$ is the part of the particles with a velocity between v and $v+dv$. In the case of thermal equilibrium $f(v)$ is the Maxwell-Boltzmann distribution function

$$f(v)dv = 4\pi\left(\frac{m}{2\pi kT}\right)^{3/2} v^2 \exp\left(-\frac{mv^2}{2kT}\right)dv \qquad \text{(B.2)}$$

with T the electron temperature and m the electron mass. This distribution is often used as an approximation. Sometimes the cross-section is given as a function of the electron energy $\varepsilon = \frac{1}{2}mv^2$. In that case we can calculate k by integrating over the electron energy distribution

$$\begin{aligned} k &= \int_0^\infty \sigma(\varepsilon) f(v) v dv = \int_0^\infty \sigma(\varepsilon) f(\varepsilon) \sqrt{\frac{2\varepsilon}{m}} \left|\frac{dv}{d\varepsilon}\right| d\varepsilon \\ &= \frac{1}{m}\int_0^\infty \sigma(\varepsilon) f(\varepsilon) d\varepsilon \end{aligned} \qquad \text{(B.3)}$$

Another cross section that plays an important part in kinetic gas theory is the so-called momentum transfer cross-section. It represents the chance that a specific particle makes a collision of any kind, weighed to the amount of momentum transferred in the collision. In the case of an electron moving in a plasma with a low ionization degree, by far the largest contribution to the momentum transfer from electrons to neutral gas particles comes from elastic collisions and the momentum transfer cross-section is also called “elastic collision cross-section”. By integration of this cross-section over the velocity distributions of the considered particles we can find the frequency for momentum transfer ν_{m}. We neglect again the velocity of the neutral particles

$$\nu_{\mathrm{m}} = N\langle\sigma_{\mathrm{m}} v\rangle = N\int \sigma_{\mathrm{m}}(v) f(v) v dv \qquad \text{(B.4)}$$

N is the density of neutral gas particles and σ_{m} the cross-section for momentum transfer.

TECHNOLOGY ASSESMENT

In this report we present a one dimensional model for micro-discharges. Micro-discharges are glow discharges on a very small scale. The distance between the electrodes is typically a few hundreds of micrometers and the gas pressure is relatively high, several hundreds of Torrs. These kinds of discharges are very interesting in connection with the newest generation of display-panels. There are several technologies for flat panel displays that make use of micro-discharges. Best known are the Plasma Display Panels (PDP's), in which the light emitted by the plasma is used to constitute the image on the screen. A totally different and less known technology is the Plasma Addressed Liquid Crystal technology (PALC). In PALC the charged particles produced in the discharge are used to charge a liquid crystal layer, and thus regulate the transparency of this layer. In this work we concentrate on the study of micro-discharges as used in PALC. The gases we consider are pure helium and helium nitrogen mixtures. We learn from the results that

- secondary emission coefficients have a strong influence on the charged particle densities developed in a discharge pulse
- the numbers of charged particles produced by the discharge pulse are amply sufficient to charge the liquid crystal layer, which ensures a homogeneous charging
- it does not really matter whether we address the data electrodes during the discharge or early in the afterglow
- the polarity of the addressing voltage might have some influence on the required addressing time, negative addressing voltages are preferable
- adding a small percentage of nitrogen shortens the helium afterglow

REFERENCES

[BAR86] M.S. Barnes, T.J. Colter, and M.E. Elta, J. Appl. Phys. **61**(1), 81 (1986)

[BLA08] A. Blanc, J. Phys. 7, 825 (1908)

[BOE87] J.P. Boeuf, Phys. Rev. A **36**(6), 2782 (1987)

[BOE94] J.P.Boeuf and L.C. Pitchford, Phys. Rev. E **51**(2), 1376 (1994)

[BOL96] BOLSIG, *Boltzmann solver for the SIGLO-series 1.0*, CPA Toulouse & Kinema Software (1996)

[BUZ90] T.S. Buzak, Information Display **10**, 7 (1990).

[BUZ93a] T.S. Buzak et al., *Achieving large area HDTV with plasma addressed liquid crystal technology*, Tektronic Report (1993)

[BUZ93b] T.S. Buzak et al., SID 93 Digest, 883 (1993)

[CHA92] Jen-Shih Chang, Y. Ichikawa, R.M. Robson, S. Matsumura, and S. Teii, J. Appl. Phys. **72**(7), 2632 (1992)

[DEL75] R. Deloche, P. Monchicourt, M. Cheret, and F. Lambert, Phys. Rev. A **13**(3), 1140 (1975)

[ELL76] H.W. Ellis, R.Y. Pai, E.W. McDaniel, E.A. Mason, and L.A. Viehland, Atomic Data and Nuclear Data Tables **17**, 177 (1976)

[HAS72] J.B. Hasted, *Physics of atomic collisions*, Butterworth (1972)

[ILC96] K.J.Ilcsin et al., SID 96 Digest (1996)

[JAN87] R.K. Janev, W.D. Langer, K. Evans, Jr., D.E.Post, *Elementary Processes in Hydrogen-Helium Plasmas*, Springer-Verlag Berlin Heidelberg New York (1987)

[MCD64] E.W. McDaniel, *Collision phenomena in ionized gases*, John Wiley & Sons, Inc., New York London Sydney (1964)

[MCF73] M. McFarland, D.L. Albritton, F.C. Fehsenfeld, E.E. Ferguson, and A.L. Schmeltekopf, J. Chem. Phys. **59**(12) (1973)

[MON70] A.R. De Monchy, *A study of the nitrogen afterglow*, thesis University of Amsterdam (1970)

[MEU95] J. Meunier, Ph. Belenguer and J.P. Boeuf, J. Appl. Phys. **74** (2), 731 (1995)

[PAC62] J.L. Pack and A.V. Phelps, Phys. Rev. **121**, 798 (1961)

[PIT81] L.C. Pitchford, ONeil, and Rumble, Phys. Rev. A **23**, 294 (1981)

[POU82] J.M. Pouvesle, A. Bouchoule, and J. Stevefelt, J. Chem. Phys. **77**(2), 817 (1982)

[RAI91] Y.P. Raizer, *Gas discharge physics*, Springer-Verlag Berlin Heidelberg New York (1991)

[STE82] J. Stevefelt, J.M. Pouvesle, and A. Bouchoule, J. Chem. Phys. **76**(8), 4006 (1982)

[SCH69] D.L. Scharfetter and H.K. Hummel, IEEE Trans. Electron. Devices **ED-16**, 64 (1969)